Elevated temperature inhibits SARS-CoV-2 replication in respiratory epithelium independently of the induction of IFN-mediated innate immune defences

Vanessa Herder[1a], Kieran Dee[1a], Joanna K. Wojtus[1], Daniel Goldfarb[1], Christoforos Rozario[1], Quan Gu[1], Ruth F. Jarrett[1], Ilaria Epifano[1], Andrew Stevenson[1], Steven McFarlane[1], Meredith E. Stewart[1], Agnieszka M. Szemiel[1], Rute M. Pinto[1], Andreu Masdefiol Garriga[1/2], Sheila V. Graham[1b], Pablo R. Murcia[1b], Chris Boutell[1b].

[1] MRC-University of Glasgow Centre for Virus Research (CVR), 464 Bearsden Road, Glasgow, G61 1QH, Scotland (UK)

[2] University of Glasgow School of Veterinary Medicine, 464 Bearsden Road, Glasgow, G61 1QH, Scotland (UK)

[a] Authors contributed equally to this work

[b] Co-corresponding authors

Corresponding author:

Chris Boutell; Email: chris.boutell@glasgow.ac.uk

Running title: Elevated temperature restricts SARS-CoV-2 replication

Keywords: Respiratory epithelium, SARS-CoV-2, primary human bronchiolar epithelial cells, COVID-19, temperature, immune regulation, RNA-Seq

Abstract

The pandemic spread of SARS-CoV-2, the etiological agent of COVID-19, represents a significant and ongoing international health crisis. A key symptom of SARS-CoV-2 infection is the onset of fever, with a hyperthermic temperature range of 38 to 41°C. Fever is an evolutionarily conserved host response to microbial infection and inflammation that can influence the outcome of viral pathogenicity and regulation of host innate and adaptive immune responses. However, it remains to be determined what effect elevated temperature has on SARS-CoV-2 tropism and replication. Utilizing a 3D air-liquid interface (ALI) model that closely mimics the natural tissue physiology and cellular tropism of SARS-CoV-2 infection in the respiratory airway, we identify tissue temperature to play an important role in the regulation of SARS-CoV-2 infection. We show that temperature elevation induces wide-spread transcriptome changes that impact upon the regulation of multiple pathways, including epigenetic regulation and lncRNA expression, without disruption of general cellular transcription or the induction of interferon (IFN)-mediated antiviral immune defences. Respiratory tissue incubated at temperatures >37°C remained permissive to SARS-CoV-2 infection but severely restricted the initiation of viral transcription, leading to significantly reduced levels of intraepithelial viral RNA accumulation and apical shedding of infectious virus. To our knowledge, we present the first evidence that febrile temperatures associated with COVID-19 inhibit SARS-CoV-2 replication. Our data identify an important role for temperature elevation in the epithelial restriction of SARS-CoV-2 that occurs independently of the induction of canonical IFN-mediated antiviral immune defences and interferon-stimulated gene (ISG) expression.

Introduction

The pandemic spread of severe acute respiratory syndrome coronavirus 2 (SARS-CoV-2, SCV2; (1-3)) is an ongoing international health crisis with over 58 million infections and 1.3 million reported deaths worldwide to date (WHO, https://covid19.who.int; November 2020). The spectrum of SCV2 related disease (COVID-19; coronavirus disease 2019) is highly variable, ranging from asymptomatic viral shedding to acute respiratory distress syndrome (ARDS), multi-organ failure, and death. Besides coughing, dyspnoea, and fatigue, fever (also known as pyrexia) is one of the most frequent symptoms of SCV2 infection (4-8). Fever is an evolutionarily conserved host response to microbial infection, which can influence the regulation of host innate and adaptive immune responses (9, 10). Unlike hyperthermia or heat stroke, fever represents a controlled shift in body temperature regulation induced by the expression of exogenous (microbial) and endogenous (host) pyrogenic regulatory factors, including PAMPS (pathogen associated molecular patterns) and pro-inflammatory cytokines (e.g. interleukin 6, IL-6) (9, 10). Body temperature naturally varies throughout the day, with age, sex, and ethnic origin being contributing factors to body temperature regulation (9, 10). In healthy middle-aged adults, fever is defined as a temperature range from 38 to 41°C (ΔT ~1-4°C above baseline), with low (38 to 39°C), moderate (39.1 to 40°C), high (40.1 to 41.1°C), and hyperpyrexia (>41.1°C) febrile temperature ranges (10). Temperature elevation confers protection against a number of respiratory pathogens (9, 11), with antipyretic drug treatment shown to increase the mortality rate of intensive care unit (ICU) patients infected with influenza A virus (IAV) (12-14).

With respect to COVID-19, up to 90% of hospitalized patients show symptoms of fever (4-8). The majority of patients display low (44%) to moderate (13 to 34%) grade fever (4, 5). COVID-19 ICU patients also show a ~10% higher prevalence of fever relative to non-ICU patients with milder disease manifestations (6, 15), suggesting fever to play a role during

71 COVID-19 disease progression. *In vitro* studies have shown that SCV2 replicates more
72 efficiently at lower temperatures associated with the upper respiratory airway (33°C), which
73 correlates with an overall weaker interferon (IFN)-mediated antiviral immune response
74 relative to core body temperatures observed in the lower respiratory airway (37°C) (16).
75 These data suggest that tissue temperature could be a significant determinant of SCV2
76 tropism and immune regulation. However, it remains to be determined what effect
77 temperature elevation above 37°C has on SCV2 infection. We therefore set out to determine
78 the net effect of elevated temperature on SCV2 infection within respiratory epithelial tissue.
79 Utilizing a three-dimensional (3D) respiratory model that closely mimics the tissue
80 physiology and cellular tropism of SCV2 infection observed in the respiratory airway of
81 COVID-19 patients (16-24), we demonstrate that elevated temperature (≥ 39°C) restricts the
82 replication and propagation of SCV2 in respiratory epithelium independently of the induction
83 of type-I (IFNβ) and type-III (IFNλ) IFN-mediated immune defences. We show that
84 respiratory epithelium remains permissive to SCV2 infection at temperatures up to 40°C, but
85 restricts viral transcription leading to significantly reduced levels of viral RNA (vRNA)
86 accumulation and apical shedding of infectious virus. Importantly, we identify temperature to
87 play an important role in the differential regulation of epithelial host responses to SCV2
88 infection, including epigenetic, long non-coding RNA (lncRNA), and immunity-related
89 pathways. Collectively, our data identify an important role for tissue temperature in the
90 epithelial restriction of SCV2 replication in respiratory tissue independently of the induction
91 of type-I and type-III IFN-mediated antiviral immune defences.
92
93

Results

Differentiation of primary human bronchial epithelial cells into ciliated respiratory epithelium supports SARS-CoV-2 replication *in vitro*. In order to establish a respiratory model suitable for studying the effect of temperature on SCV2 replication, we differentiated primary human bronchiolar epithelial (HBE) cells (isolated from a male Caucasian donor aged 63 years) into pseudostratified respiratory epithelium. Haematoxylin and Eosin (H&E) and immunohistochemistry (IHC) staining of respiratory airway cultures demonstrated that these tissues to contain a mixture of epithelial and goblet cells, with significant levels of apical ciliation and expression of ACE2 (Figure 1A), the principal surface receptor for SCV2 and major determinant of tissue tropism (25-28). Infection of respiratory airway cultures with SCV2 (strain England 2; 10^4 PFU/tissue) at 37°C demonstrated that these tissues support SCV2 infection and replication, with intraepithelial and apical vRNA accumulation detectable by *in situ* hybridization by 96 h post-infection (Figure 1A). Notably, we observed discrete clusters of SCV2 RNA accumulation within the respiratory epithelium, indicative of SCV2 cell-type specific tropism and/or localized patterns of immune restriction (see below; (29, 30)). The overall morphology of the respiratory epithelium remained largely intact, with little to no discernible shedding of the ciliated surface epithelium over the time course of infection (Figure 1A). Measurement of genome copies (RT-qPCR) and infectious virus ($TCID_{50}$) within apical washes collected over time (24 to 144 h) demonstrated the linear phase of virus shedding to occur between 48 and 96 h, with peak titres at 120 h post-infection (Figure 1B to E).

In order to determine which cellular pathways were modulated in response to SCV2 infection, we performed RNA-Seq analysis on RNA extracted from mock-treated or SCV2-infected respiratory cultures incubated at 37°C for 72 h, a time point in the linear phase of viral shedding (Figure 1C to E). Out of the 787 differentially expressed genes (DEGs) (Figure

2A, Supplemental File S1; $p<0.05$, ≥ 1.5 or ≤ -1.5 log2 Fold Change [log2 FC]), pathway analysis identified DEG enrichment in immune system and cytokine related pathways to be significantly upregulated in SCV2-infected relative to mocked-treated tissues (Figure 2B, C $p<0.0001$). Type-I (IFNβ, *IFNB1*) and type-III (IFNλ, *IFNL1-3*) IFNs, along with a subset of interferon stimulated genes (ISGs; e.g. *BST2*, *ISG15*, *Mx1*, and *ZBP1* amongst others), and other pro-inflammatory cytokines (*IL6 and IL32*) were upregulated (Figure 2D). Indirect immunofluorescence staining of tissue sections demonstrated that induced ISG expression coincided with productively infected areas of the respiratory epithelium (Figure 2E, Mx1), identifying localized areas of immune regulation within infected tissue. Our findings are consistent with previous reports showing that SCV2 infection induces an IFN-mediated antiviral immune response upon infection of epithelial tissue (16, 18-21, 30-32).

Respiratory airway cultures induce a heat stress response at elevated temperature. We next investigated the influence of temperature on our respiratory epithelium model. Mock treated respiratory cultures were incubated at 37, 39, or 40°C (representative of core body temperature and low to moderate grade febrile temperatures, respectively) for 72 h prior to tissue fixation or RNA extraction and RNA-Seq. H&E staining demonstrated no obvious morphological changes to the respiratory epithelium upon incubation at elevated temperature (Figure 3A), although an increase in epithelium thickness was detected relative to tissues incubated at 37°C (Figure 3B; 39°C $p<0.0001$, 40°C $p<0.0001$). RNA-Seq analysis demonstrated no difference in the expression level of ACE2 (Figure 3C; $p=0.4001$) or a reference set of genes known to be constitutively expressed across a wide range of cell types and tissues (Figure 3D; 24 genes, $p=0.9106$; (33-35)). These data indicate that cellular transcription remains largely unperturbed at elevated temperatures up to 40°C. Out of the 650 DEGs identified (Figure 3E, Supplemental File S2; $p<0.05$, ≥ 1.5 or ≤ -1.5 log2 FC), pathway

144 analysis identified DEG enrichment in multiple pathways in tissues incubated at 40°C
145 relative to 37°C, including meiotic recombination, DNA methylation, rRNA expression, and
146 collagen metabolism (Figure 3F). DEG enrichment was also observed in cellular pathways
147 relating to heat stress (Figure 3F black arrow, 3G; R-HSA-3371556) and cellular response to
148 external stimuli (Figure 3G; R-HSA-8953897). Analysis of complete gene sets associated
149 with the cellular response to heat stress (Figure 3H, p=0.0013) or cellular response to heat
150 (Figure S1, p=0.0018; GO:0034605) identified that these pathways were upregulated in
151 respiratory tissues incubated at 40°C relative to 37°C (Supplemental File S2). We conclude
152 that our respiratory tissue model induces a heat stress response at elevated temperature
153 without visible damage to the epithelium or induction of IFN-mediated antiviral immune
154 defences.
155
156 **Elevated temperature restricts the replication of SARS-CoV-2 in respiratory airway**
157 **cultures.** We next examined the effect of temperature on SCV2 replication in our 3D tissue
158 model. Respiratory cultures were incubated at 37, 39, or 40°C for 24 h prior to mock
159 treatment or SCV2 infection and continued incubation at their respective temperatures.
160 Measurement of genome copies and infectious virus within apical washes collected over time
161 (24 to 72 h) demonstrated that extracellular SCV2 titres were significantly decreased at both
162 39 and 40°C relative to 37°C (Figure 4A to D). RT-qPCR analysis of RNA isolated from
163 infected tissues at 72 h post-infection demonstrated significantly lower levels of intracellular
164 vRNA in tissues incubated at 39 or 40°C (Figure 4E; 39°C p=0.0278, 40°C p=0.0033). These
165 data indicate that respiratory tissue remains permissive to SCV2 infection (tissue entry) but
166 refractory to SCV2 replication at elevated temperatures ≥39°C. To our knowledge, these data
167 identify for the first-time a temperature-dependent growth defect in SCV2 replication at
168 elevated temperature (>37°C).

In order examine the underlying mechanism(s) of this intracellular restriction, we compared the relative DEG profiles ($p<0.05$, ≥ 1.5 or ≤ -1.5 log2 FC) from mock-treated or SCV2-infected tissues at 37 or 40°C (Figure 5, S2, S3, Supplemental Files S1 to S4). Distinct patterns of DEG expression were detected between each paired condition analyzed (Figure 5A, B; Supplemental File S5), with clusters of gene commonality (Figure 5B, purple lines) or shared gene pathway ontology (Figure 5B, blue lines). We also identified lncRNAs and micro-RNAs (miRNAs) to be differentially expressed between temperature and SCV2 infection conditions (Figure S4; Supplemental File S6). Pathway analysis identified DEG enrichment to be highly specific for each paired condition analyzed, with a clear enrichment in immunity related pathways at 37°C relative to all other conditions (Figure 5C). These data indicate that tissue temperature plays an important role in the differential regulation of transcriptional host responses to SCV2 infection of epithelial tissue. To examine the influence of temperature on immune regulation further, we directly compared the transcriptome profiles from SCV2 infected tissues at 37 and 40°C. Out of the 859 DEGs identified (Figure 6A; $p<0.05$, ≥ 1.5 or ≤ -1.5 log2 FC), pathway analysis identified immune system and cytokine related pathways to be suppressed during SCV2 infection at 40°C relative to 37°C (Figure 6B, C; Supplemental File S7), findings consistent with a failure of SCV2 to induce the expression of type-I (INFβ, *IFNB1*) or type-III (IFNλ, *IFNL1-3*) IFNs at 40°C (Figure 6D). Analysis of this subset of differentially expressed immune genes identified a decrease in gene expression during SCV2 infection at 40°C (mean log2 counts per million [CPM] 1.147, SD 3.656) relative to mock treatment at 37°C (mean log2 CPM 1.578, SD 3.716; Figure 6C). These data suggest that SCV2 infection of respiratory tissue at 40°C is not sufficient to induce a robust innate immune response, indicating that the observed temperature restriction of SCV2 at elevated temperature occurs independently of IFN-mediated antiviral immune defences.

194 In order to substantiate these findings, we examined the influence of temperature on
195 SCV2 replication in VeroE6 cells, a cell line derived from *Chlorocebus Sabaeus* (African
196 green monkey) known to be permissive to SCV2 infection but defective in type-I IFN-
197 mediated immune defences (26, 36, 37). SCV2 replication was restricted at 40°C, but not
198 39°C, relative to infection at 37°C with or without elevated temperature pre-incubation
199 (Figure 7A to C). Transcriptomic analysis revealed significant differences in the baseline
200 expression of genes associated with the cellular response to heat pathway (GO:0034605)
201 between respiratory tissue and undifferentiated HBE ($p=0.0142$) or VeroE6 ($p<0.0001$) cells
202 (Figure 7D, E), but not a reference set of genes expressed across a wide range of cell types
203 and tissues (Figure 7F, G, Supplemental File S8; (33-35)). We posit that such differences in
204 the constitutive expression of heat stress response genes is likely to influence the relative
205 restriction of SCV2 upon temperature elevation in a cell type, and potentially species-
206 specific, dependent manner. These data support our tissue analysis (Figure 4 to 6), which
207 demonstrates that the temperature-dependent restriction of SCV2 to occur independently of
208 the induction of IFN-mediated antiviral immune defences.
209 We next examined the stage at which SCV2 infection became restricted during
210 infection of respiratory tissue at elevated temperature. RNA-Seq analysis of SCV2 infected
211 tissues at 72 h post-infection demonstrated no significant difference in the total number of
212 mapped reads (human + SCV2) between 37 and 40°C (Figure 8A, $p=0.3429$). However,
213 analysis of viral reads identified a decrease in the relative abundance of viral transcripts
214 mapping to multiple ORFs upon temperature elevation (Figure 8B to D, $p<0.0010$). Indirect
215 immunofluorescence staining of tissue sections for SCV2 nucleocapsid (N) expression
216 demonstrated significantly fewer clusters of SCV2 positive cells within infected tissues at
217 40°C relative to 37°C (Figure 8E, F, $p=0.0022$). We conclude that infection of respiratory
218 tissue at elevated temperature restricts SCV2 replication through a mechanism that inhibits

219 viral transcription independently of the induction of IFN-mediated antiviral immune defences
220 that have been reported to restrict SCV2 propagation and spread (31, 38).
221

222 ## Discussion

223 A defining symptom of COVID-19 is the onset of fever with a febrile temperature range of
224 38 to 41°C (4-8). However, the effect of elevated temperature on SCV2 tissue tropism and
225 replication has remained to be determined. Here we identify a temperature-sensitive
226 phenotype in SCV2 replication in respiratory epithelial tissue that occurs independently of
227 the induction of IFN-mediated innate immune defences known to restrict SCV2 replication
228 (31, 38). The differentiation of pseudostratified respiratory epithelium has proven to be a
229 valuable research tool to investigate the cellular tropism, replication kinetics, and immune
230 regulation of SCV2 infection, as these tissue models mimic many aspects of infection
231 observed in animal models and COVID-19 patients (16-24, 29, 32, 39-42). While the use of
232 such 3D models represents an important advancement over traditional 2D cell culture
233 systems, the absence of circulating immune cells (e.g. macrophages, natural killer cells,
234 dendritic cells, and neutrophils) which modulate fever and pro-inflammatory immune
235 responses to microbial infection is an important limiting factor (9, 10, 43). Thus, we limit our
236 conclusions to the effect of elevated temperature on SCV2 infection and replication within
237 the respiratory epithelium. Additional animal studies are warranted to determine the overall
238 net effect of fever and pro-inflammatory immune responses on body temperature
239 thermoregulation and its corresponding influence on SCV2 tissue tropism and replication *in*
240 *vivo*.

241 Consistent with previous reports (16, 18-21, 30-32), SCV2 infection of respiratory
242 epithelium induced a pro-inflammatory immune response (Figure 2; IFNβ, IFNλ1-3, and IL-
243 6). While SCV2 has been reported to induce a relatively weak IFN immune signature in

244 comparison to other respiratory viruses (e.g. IAV) (20, 44), we regularly observed localized
245 areas of epithelial infection (Figure 1A, 2E, 8E) that were coincident with elevated levels of
246 ISG expression (Figure 2E, Mx1). Our findings are consistent with reports that have shown
247 similar patterns of localized infection in the respiratory airway of SCV2 infected ferrets and
248 surface epithelium of organoid cultures (29, 30, 32, 45). These data indicate that SCV2
249 induces a localized immune response during the opening phase of productive infection that is
250 likely to restrict the progress of infection through the epithelium (Figure 1A) (30, 31, 38).
251 Thus, differences in the proportion of epithelial infection and/or rate of intraepithelial spread
252 may account for the observed differences in immune signatures between different respiratory
253 pathogens (20, 46) and variance in apical yields of infectious virus at any given time point of
254 analysis (Figure 1B and Figure 4B, D). As we observed localized areas of ISG induction
255 (Figure 2E), our data support a model of epithelial infection where receptor-binding
256 consumption kinetics of secreted IFN may limit cytokine diffusion and the intraepithelial
257 induction of innate immune defences prior to the recruitment of immune cells and IFNγ
258 secretion (47, 48).

259 We demonstrate that respiratory epithelial cultures induce a significant heat stress
260 response upon temperature elevation without significant loss of tissue integrity, disruption to
261 cellular transcription, diminished levels of ACE2 expression, or DAMP (damage associated
262 molecular pattern) activation of immune defences at temperatures up to 40°C (Figure 3).
263 Importantly, the elevation of temperature alone was not sufficient to inhibit SCV2 entry into
264 respiratory tissue (Figure 4E), but restricted SCV2 replication leading to reduced levels of
265 SCV2 apical shedding (Figure 4A to D). Thus, we identify tissue temperature to play an
266 important role in the epithelial restriction of SCV2 replication. To our knowledge, these data
267 represent the first account of a growth defect in SCV2 replication at febrile temperatures
268 >37°C. Transcriptomic analysis identified substantial differences in the relative degree of

269 immune activation in respiratory tissue infected at 40°C (Figure 5 and 6), despite these
270 tissues having abundant levels of intracellular vRNA (Figure 4E). We posit that the lack of
271 immune induction observed at 40°C is likely a consequence of diminished levels of SCV2
272 replication, as vRNA replication has previously been shown to play an important role in the
273 production of PAMPs, including dsRNA intermediates, required for PRR detection and the
274 activation of innate immune defences during respiratory virus infection (49-52). We also
275 show the thermal restriction of SCV2 replication to occur in VeroE6 cells, a cell line
276 permissive to SCV2 infection but defective in type-I IFN-mediated antiviral immune
277 defences (26, 36, 37). Thus, we conclude that elevated temperature restricts SCV2 replication
278 independently of the induction of ISG expression. Importantly, however, PRR detection of
279 PAMPs which stimulate the production and secretion of pro-inflammatory cytokines
280 (including IL-6) is a pre-requisite requirement for a fever response to microbial challenge *in*
281 *vivo* (9, 10). Thus, additional animal studies are warranted to determine if the temperature
282 restriction of SCV2 observed in respiratory cultures can occur independently of IFN-
283 mediated immune defences *in vivo*. While speculative, we posit that low to moderate grade
284 fever may confer protection to respiratory tissue within SCV2 infected individuals as a
285 component of a homeostatically controlled non-hyperinflammatory immune response to
286 infection.

287 While we identify temperature to play an important role in the regulation of SCV2
288 replication in respiratory epithelia, the precise mechanism(s) of restriction remains to be
289 determined and warrants further investigation. The induction of a heat stress response alone
290 within respiratory tissue may be sufficient to limit SCV2 replication (Figure 2, Figure S3), as
291 the activation and/or induction of stress response proteins has been shown to play both a
292 positive (proviral) and negative (antiviral) role in the replication of many viruses (53-55).
293 Our transcriptomic analysis identified epithelial host responses to be differentially regulated

294 in response to both temperature elevation and SCV2 infection (Figure 5 and 6), with unique
295 profiles of induced gene expression between mock and SCV2 infected tissues at elevated
296 temperature (Figure 5, Figure S2). Thus, SCV2 infection of respiratory epithelia at elevated
297 temperature elicits a distinct host response that may directly contribute to the restriction of
298 SCV2 propagation, for example the induction of mucins (Figure S2, *MUC4* and *MUC5AC*)
299 which have been proposed to limit coronavirus disease progression and IAV replication (56,
300 57). We also identified a significant difference in the differential expression of lncRNAs and
301 miRNAs upon temperature elevation and SCV2 infection that warrants additional
302 investigation (Figure S4), as changes in the relative expression of non-coding RNAs are
303 known to influence the outcome of virus infection independently of IFN-mediated immune
304 defences (58). Thus, multiple gene products and/or pathways may contribute to the sequential
305 or accumulative restriction of SCV2 replication within respiratory tissue at elevated
306 temperature.

307 Importantly, we identify elevated temperature to lead to lower levels of SCV2
308 transcription and vRNA accumulation (Figure 4E, Figure 8D), suggesting that the
309 temperature-dependent block in SCV2 propagation occurs prior to and/or during vRNA
310 replication. We hypothesize that this block in transcription/replication may relate to the
311 inhibition of SCV2 RNA-dependent RNA-polymerase (RdRp) activity or RdRp RNA
312 binding affinity at elevated temperature, as the genomic replication activity of the IAV RdRp
313 polymerase is known to be restricted at elevated temperature (41°C) (59). Notably, IAV cold-
314 adaptation of RdRp activity has been shown to be a host determinant for avian IAV zoonosis,
315 which naturally replicate at higher temperatures (41°C) within the intestinal tracts of birds
316 (60). As circulating clinical strains of SCV2 are susceptible to non-synonymous mutations
317 within RdRp coding sequences (http://cov-glue.cvr.gla.ac.uk/#/home), detailed molecular
318 studies are warranted to determine if such amino acid substitutions influence the thermal

restriction of SCV2 replication. To our knowledge, no temperature sensitive growth defect for coronaviruses has been reported to date, although a temperature-sensitive (ts) coronavirus mutant has been identified for murine hepatitis virus (MHV, tsNC11) (61). The replication defect of tsNC11 was attributed to coding substitutions within the macrodomain and papain-like protease 2 domain of the non-structural protein 3, which displayed a severe growth defect at 40°C in DBT (Delayed Brain Tumor) cells, whereas wild-type MHV replicated to equivalent titres at 40°C to those observed at 37°C (61). Thus, we present the first evidence demonstrating that a circulating clinical strain of coronavirus is sensitive to temperature thermoregulation. As such, heat-adaptation gain of function experiments through serial passage of SCV2 in respiratory cultures incubated at ≥39°C may shed light on whether the temperature restriction of SCV2 observed is related to viral or cellular host factors, although appropriate levels of biosafety (ethical and genetic modification) should be considered prior to such experimentation.

In summary, we identify an important role for tissue temperature in the restriction of SCV2 replication in respiratory epithelia that occurs independently of the induction of IFN-mediated antiviral immune defences. We demonstrate tissue temperature to significantly influence the differential regulation of epithelial host responses induced in response to SCV2 infection. Future investigation is warranted to determine the precise mechanism(s) of restriction, as this may uncover novel avenues for therapeutic intervention in the treatment of COVID-19.

Materials and Methods

Virus

Severe Acute Respiratory Syndrome Virus-2 (SARS-CoV-2, SCV2) BetaCoV/England/02/2020/EPI_ISL_407073 was isolated from a COVID-19 patient (a gift from Public Health England). The virus was passaged three times in VeroE6 cells and genotype sequence confirmed by Illumina sequencing. All experiments were performed in a Biosafety level 3-laboratory at the MRC-University of Glasgow Centre for Virus Research (SAPO/223/2017/1a).

SCV2 replication kinetics in VeroE6 cells

VeroE6 cells (a gift from Michelle Bouloy, Institute Pasteur, France) were propagated in Dulbecco's Modified Eagle Medium (DMEM GlutaMAX; ThermoFisher, 31966-021) supplemented with 10% fetal calf serum (FCS; ThermoFisher, 10499044 [Lot Number 08G8293K]) at 37°C with 5% CO_2. Cells were seeded the day before infection at a density of $2x10^5$ cells per well in a 12-well plate and infected with 10^4 PFU of SCV2 diluted in serum-free DMEM for 120 minutes (mins) with occasional rocking. The inoculum was removed and replaced by DMEM + 10% FCS. Supernatant was collected every 24 hours (h) and snap-frozen prior to analysis. For temperature inhibition experiments, cells were either pre-incubated at 37, 39, or 40°C for 24 h prior to infection with continued incubation at their respective temperatures or incubated at the indicated temperatures after the addition of the medium.

Differentiation of respiratory epithelium

Primary human bronchiolar epithelial (HBE) cells from a healthy 63-year-old white Caucasian male (non-smoker) were sourced from Epithelix Sarl (Geneva, Switzerland). Cells were propagated at 37°C with 5% CO_2 in hAEC culture medium (Epithelix, EP09AM). All differentiation experiments were performed on cells that had been passaged a total of four

times. Cells were seeded onto transwells (Falcon, 734-0036) at a cell density of $3x10^4$ cells per transwell and grown to confluency. Cells were differentiated under air-liquid interface (ALI) in PneumaCult-ALI medium containing hydrocortisone and heparin supplements (STEMCELL Technologies, 05001) as specified by the manufacturer's guidelines. Cells were differentiated for a minimum of 35 days, with media changed every 48 h and twice weekly apical washing in serum-free DMEM after day 20 at ALI. ALI cultures were apically washed twice before infection, 24 h prior to infection and immediately preceding infection. Cultures were inoculated apically with 100 µl of serum-free DMEM containing 10^4 PFU of SCV2 (based on VeroE6 titres) for 120 mins. The inoculum was removed, and the apical surface washed once in serum-free DMEM (0 h time point). Unless stated otherwise, ALI cultures were incubated at 37°C with 5% CO_2. For temperature inhibition experiments, ALI cultures were pre-incubated at 37, 39, or 40°C for 24 h prior to infection with continued incubation at their respective temperatures. Apical washing for 30 mins in 200 µl of serum-free DMEM was used to collect infectious virus. Supernatants were divided into two 100 µl aliquots; one for virus quantitation ($TCID_{50}$) and the other for vRNA extraction in TRIzol (ThermoFisher, 15596026; 1 in 3 dilution). Samples were stored at -80°C until required. Tissues were fixed at the indicated time points in 8% formaldehyde (Fisher Scientific, F/1501/PB17) for 16 to 24 h prior to paraffin embedding and processing.

$TCID_{50}$

VeroE6 cells (subclone 6F5, MESO) were seeded the day before infection into 96-well-plates at a density of $1.1x10^5$ cells/well in DMEM + 10% FCS at 37°C with 5% CO_2. Virus supernatants were serially diluted 1:10 in DMEM + 2% FCS in a total volume of 100 µl. Cells were infected in triplicate and incubated for three days at 37°C with 5% CO_2. The inoculum was removed and fresh media overlayed. Plates were incubated for three days at 37°C in 5% CO_2. Cells were fixed in 8% formaldehyde (Fisher Scientific, F/1501/PB17) for

≥ 2.5 h. Cytopathic effect was scored by staining with 0.1% Coomassie Brilliant Blue (BioRad, 1610406) in 45% methanol and 10% glacial acetic acid. $TCID_{50}$ was calculated according to Reed–Muench and Spearman–Kärber as described (62).

Plaque assay

VeroE6 cells were seeded at a density of $2.5x10^5$ cells/well in 12-well plates the day before infection. Ten-fold serial dilutions of virus were prepared in DMEM + 2% FCS in a total volume of 500 µl. Cells were infected for 60 mins with occasional rocking at 37°C in 5% CO_2. The inoculum was removed and 1 ml of overlay containing 0.6% Avicel (Avicel microcrystalline cellulose, RC-591) made up in DMEM containing 2% FCS was added to each well. Cells were incubated for three days at 37°C in 5% CO_2 prior to fixation in 8% formaldehyde and Coomassie brilliant blue staining (as described above). Plaques were counted manually and the plaque forming unit (PFU) per ml calculated.

Reverse transcription quantitative PCR (RTq-PCR)

RNA was extracted from TRIzol treated apical wash samples using a QIAGEN RNeasy Mini kit (Qiagen, 74106) following the manufacture's protocol. SCV2 RNA was quantified using a NEB Luna Universal Probe One-Step RT-qPCR Kit (New England Biolabs, E3006) and 2019-nCoV CDC N1 primers and probes (IDT, 10006713). Genome copy numbers were quantified using a standard curve generated from serial dilutions of an RNA standard used throughout the study. The RNA standard was calibrated using a plasmid (2019-nCoV_N; IDT, 10006625) that was quantified using droplet digital PCR. Values were normalized to copies/ml for apical washes or copies/tissue for cell-associated RNA.

***In situ*-hybridization and immunostaining of respiratory tissue sections**

Paraffin-embedded tissues were sectioned using a microtome (~2-3 µm thick) and mounted on glass slides. Tissue sections were stained with Haematoxylin and Eosin (H&E). For immunofluorescence staining, tissue sections underwent antigen retrieval by citrate (pH 6) or

EDTA (pH 8) pressure cooking (as indicated). RNAscope was used for the detection of SCV2 RNA using a Spike-specific probe set (Advanced Cell Diagnostics, 848561 and 322372) following the manufacturer's protocol, which included a pre-treatment with boiling in target solution and proteinase K treatment. ACE2 was detected using a rabbit polyclonal anti-hACE2 antibody (Cell Signalling, 4355S; citrate antigen-retrieval) and EnVision+ anti-rabbit HRP (Agilent, K4003). Slides were scanned with a bright field slide scanner (Leica, Aperio Versa 8). Mx1 was detected using a mouse monoclonal anti-Mx1 antibody ((63); EDTA antigen-retrieval). SCV2 nucleocapsid protein was detected using a sheep polyclonal anti-SCV2 N protein antibody (University of Dundee, DA114; EDTA antigen-retrieval). Secondary antibodies for detection were rabbit anti-sheep AlexaFluor 555 (abcam, ab150182) and rabbit anti-mouse AlexaFluor 488 (Sigma-Aldrich, SAB4600056). Nuclei were stained with ProLong Gold (Life Technologies, P36941). Images were collected using a Zeiss LSM 710 confocal microscope using 40x Plan-Apochromat oil objective lens (numerical aperture 1.4) using 405, 488, and 543 nm laser lines. Zen black software (Zeiss) was used for image capture and exporting images, with minimal adjustment (image rotation) in Adobe Photoshop for presentation.

Tissue section image analysis

Scanned Haematoxylin and Eosin (H&E) stained sections were analyzed using Aperio ImageScope analysis software (Leica). Epithelial thickness was measured by manually outlining the bottom and top surfaces of each epithelium (excluding cilia) and measuring the vertical point-to-point distance between each surface across the epithelium. One hundred evenly distributed distance measurements were acquired per epithelium per experimental condition in triplicate.

RNA sequencing (RNA-Seq)

Transwell tissue or undifferentiated cells seeded into 12-well dishes at a cell density of $2x10^5$ cells per well were harvested by scraping into TRIzol Reagent and transferred into tubes containing 2.8 mm ceramic beads (Stretton Scientific, P000916-LYSK0-A.0). Samples were homogenized (two 20 sec pulses with a 30 sec interval at room temperature, RT) using a Percellys Cryolys Evolution Super Homogeniser (Bertin Instruments, P000671-CLYS2-A) at 5500 rounds per minute. The homogenised suspension was loaded into QIAshredder tubes (Qiagen, 79654) and centrifuged (12,000 x g for 2 mins at RT). 0.25 ml of chloroform (VWR Life Sciences, 0757) was added to the eluate and incubated at RT for 7 mins prior to centrifugation (12'000 x g, 15 minutes, 4°C). The aqueous phase was transferred into a fresh tube, mixed with 250 µl of 100% ethanol, and RNA isolated using RNAeasy columns (Qiagen, 74104) following the manufacturer's protocol, that included a 15 min DNAse treatment (Qiagen, 79254) treatment at RT. Eluted RNA was quantified using a NanoDrop 2000 Spectrophotometer (ThermoFisher Scientific, ND-2000) and quality controlled on a TapeStation (Agilent Technologies, G2991AA). All samples had a RIN score of ≥ 9. One microgram of total RNA was used to prepare libraries for sequencing using an Illumina TruSeq Stranded mRNA HT kit (Illumina, 20020594) and SuperScript2 Reverse Transcriptase (Invitrogen, 18064014)
according to the manufacturer's instructions. Libraries were pooled in equimolar concentrations and sequenced using an Illumina NextSeq 500 sequencer (Illumina, FC-404-2005). At least 95% of the reads generated presented a Q score of ≥ 30. RNA-Seq reads were quality assessed (FastQC; http://www.bioinformatics.babraham.ac.uk/projects/fastqc) and sequence adaptors removed (TrimGalore; https://www.bioinformatics.babraham.ac.uk/projects/trim_galore/). RNA-Seq reads were aligned to the *Homo sapiens* genome (GRCh38) or *Chlorocebus Sabaeus* genome (ChlSab1.1), downloaded via Ensembl using HISAT2. HISAT2 is a fast and sensitive splice

aware mapper, which aligns RNA sequencing reads to mammalian-sized genomes using FM index strategy (64). RNA-Seq reads were also mapped to SARS-CoV-2 (GISAID accession ID:EPI_ISL_407073) using Bowtie2 (65). FeatureCount (66) was used to count reads mapping to gene annotation files. Reads counts were normalized to counts per million (CPM) unless otherwise stated. The edgeR package was used to calculate the gene expression level and to analyze differentially expressed genes between sample groups (67). Sequences have been deposited in the European Nucleotide Archive (https://www.ebi.ac.uk/ena/browser/home), accession number PRJEB41332. Only high confidence ($p<0.05$) differentially expressed genes (DEGs; ≥ 1.5 or ≤ -1.5 log2 fold change, log2 FC) were used for pathway analysis in Reactome (https://reactome.org) (68, 69) or differential pathway enrichment in Metascape (https://metascape.org/gp/index.html#/main/step1) (70). In Reactome, the gene mapping tool was used as a filter to identify pathways enriched (over-represented) for mapped DEG entities. FDR (False Discovery Rate) values <0.05 were considered significant for pathway enrichment. In Metascape, all DEGs were used for differential pathway analysis. Pathway p-values <0.05 were considered significant. Differential expressed ($p<0.05$, ≥ 1.5 or ≤ -1.5 log2 FC) lncRNAs and miRNAs were identified using the Ensembl BioMart tool (http://www.ensembl.org/biomart/martview/05285d5f063a05a82b8ba71fe18a0f18). Heat maps were plotted in GraphPad Prism (version 9). Mean counts per million (CPM) values of zero were normalized to 0.01 for log2 presentation. Venn diagrams were plotted using http://bioinformatics.psb.ugent.be/webtools/Venn/.

Statistical analysis

GraphPad Prism (version 9) was used for statistical analysis. For unpaired non-parametric data, a Kruskal-Wallis one-way ANOVA or Mann-Whitney *U*-test was applied. For paired non-parametric data, a one-way ANOVA Friedman test or Wilcoxon matched-pairs sign rank

493 test was applied. Statistical p-values are shown throughout. Statistically significant
494 differences were accepted at $p \leq 0.05$.

495

496 Acknowledgements

497 The authors thank Lynn Marion Stevenson, Frazer Bell, and Lynn Oxford (College of
498 Medical, Veterinary and Life Sciences, University of Glasgow) for their exceptional efforts
499 during the UK lockdown. VH was funded by the German Research Foundation (Deutsche
500 Forschungsgemeinschaft; project number 406109949) and the Federal Ministry of Food and
501 Agriculture (BMEL; Förderkennzeichen: 01KI1723G). KD and PRM were funded by the
502 Medical Research Council (MRC; MC_UU_12014/9 to PRM). JW was funded by an MRC
503 CVR DTA award (MC_ST_U18018). DG was funded by an MRC-DTP award
504 (MR/R502327/1). CR was funded by a BBSRC-CTP award (BB/R505341/1). QG was
505 funded by the MRC (MC_UU_12014/12). IE was funded by a CSO project grant
506 (TCS/19/11). MES was funded by the MRC (MC PC 19026). AMS was funded by a
507 UKRI/DHSC grant (BB/R019843/1 to Brian Willett, MRC-UoG CVR) and MRC CoV
508 supplement grant (MC_PC_19026). RMP was funded by the MRC (MC_UU_12014/10).
509 AMG was funded by studentship awards from the University of Glasgow School of
510 Veterinary Medicine (Georgina D. Gardner, 145813; John Crawford, 123939). CB and SMF
511 were funded by the MRC (MC_UU_12014/5 to CB).

512

513 Availability of data

514 The datasets generated and analyzed during the current study are available in the University
515 of Glasgow data repository (a doi will be generated upon manuscript acceptance). RNA-Seq

data sets are available from the European Nucleotide Archive, accession number PRJEB41332 (available upon manuscript acceptance).

Author contributions

VH, KD (joint first authors): Conceptualization, Data curation, Formal Analysis, Investigation, Methodology, Project administration, Validation, Visualization, Writing – original draft, Writing – review & editing.

JKW, RJ, CR, DG, IE, AS, SMF, QG: Data curation, Formal Analysis, Investigation, Methodology, Validation

MS, AMS, RMP.: Resources, Methodology

AMG: Data curation, Formal Analysis

SG, PRM: Conceptualization, Funding acquisition, Methodology, Supervision, Writing – review & editing.

CB: Conceptualization, Methodology, Data curation, Formal Analysis, Investigation, Funding acquisition, Project administration, Supervision, Validation, Writing – Original draft, Writing – review & editing.

Conflicts of interest

The authors declare no conflict of interest.

References

1. Zhu N, Zhang D, Wang W, Li X, Yang B, Song J, et al. A Novel Coronavirus from Patients with Pneumonia in China, 2019. N Engl J Med. 2020;382(8):727-33.
2. Lu R, Zhao X, Li J, Niu P, Yang B, Wu H, et al. Genomic characterisation and epidemiology of 2019 novel coronavirus: implications for virus origins and receptor binding. Lancet. 2020;395(10224):565-74.
3. Wu F, Zhao S, Yu B, Chen YM, Wang W, Song ZG, et al. A new coronavirus associated with human respiratory disease in China. Nature. 2020;579(7798):265-9.
4. Huang C, Wang Y, Li X, Ren L, Zhao J, Hu Y, et al. Clinical features of patients infected with 2019 novel coronavirus in Wuhan, China. Lancet. 2020;395(10223):497-506.
5. Guan WJ, Ni ZY, Hu Y, Liang WH, Ou CQ, He JX, et al. Clinical Characteristics of Coronavirus Disease 2019 in China. N Engl J Med. 2020;382(18):1708-20.
6. Fu L, Wang B, Yuan T, Chen X, Ao Y, Fitzpatrick T, et al. Clinical characteristics of coronavirus disease 2019 (COVID-19) in China: A systematic review and meta-analysis. J Infect. 2020;80(6):656-65.
7. Hoang A, Chorath K, Moreira A, Evans M, Burmeister-Morton F, Burmeister F, et al. COVID-19 in 7780 pediatric patients: A systematic review. EClinicalMedicine. 2020;24:100433.
8. Xu T, Chen C, Zhu Z, Cui M, Chen C, Dai H, et al. Clinical features and dynamics of viral load in imported and non-imported patients with COVID-19. Int J Infect Dis. 2020;94:68-71.
9. Evans SS, Repasky EA, Fisher DT. Fever and the thermal regulation of immunity: the immune system feels the heat. Nat Rev Immunol. 2015;15(6):335-49.
10. Ogoina D. Fever, fever patterns and diseases called 'fever'--a review. J Infect Public Health. 2011;4(3):108-24.
11. Foxman EF, Storer JA, Fitzgerald ME, Wasik BR, Hou L, Zhao H, et al. Temperature-dependent innate defense against the common cold virus limits viral replication at warm temperature in mouse airway cells. Proc Natl Acad Sci U S A. 2015;112(3):827-32.
12. Earn DJ, Andrews PW, Bolker BM. Population-level effects of suppressing fever. Proc Biol Sci. 2014;281(1778):20132570.
13. Schulman CI, Namias N, Doherty J, Manning RJ, Li P, Elhaddad A, et al. The effect of antipyretic therapy upon outcomes in critically ill patients: a randomized, prospective study. Surg Infect (Larchmt). 2005;6(4):369-75.
14. Ryan M, Levy MM. Clinical review: fever in intensive care unit patients. Crit Care. 2003;7(3):221-5.
15. Cao Z, Li T, Liang L, Wang H, Wei F, Meng S, et al. Clinical characteristics of Coronavirus Disease 2019 patients in Beijing, China. PLoS One. 2020;15(6):e0234764.
16. V'kovski P, Gultom M, Steiner S, Kelly J, Russeil J, Mangeat B, et al. Disparate temperature-dependent virus – host dynamics for SARS-CoV-2 and SARS-CoV in the human respiratory epithelium. 2020.
17. Zhu N, Wang W, Liu Z, Liang C, Wang W, Ye F, et al. Morphogenesis and cytopathic effect of SARS-CoV-2 infection in human airway epithelial cells. Nat Commun. 2020;11(1):3910.
18. Chua RL, Lukassen S, Trump S, Hennig BP, Wendisch D, Pott F, et al. COVID-19 severity correlates with airway epithelium-immune cell interactions identified by single-cell analysis. Nat Biotechnol. 2020;38(8):970-9.
19. Ravindra NG, Alfajaro MM, Gasque V, Wei J, Filler RB, Huston NC, et al. Single-cell longitudinal analysis of SARS-CoV-2 infection in human bronchial epithelial cells. bioRxiv. 2020.

585 20. Blanco-Melo D, Nilsson-Payant BE, Liu WC, Uhl S, Hoagland D, Moller R, et al.
586 Imbalanced Host Response to SARS-CoV-2 Drives Development of COVID-19. Cell.
587 2020;181(5):1036-45 e9.
588 21. Pizzorno A, Padey B, Julien T, Trouillet-Assant S, Traversier A, Errazuriz-Cerda E,
589 et al. Characterization and Treatment of SARS-CoV-2 in Nasal and Bronchial Human
590 Airway Epithelia. Cell Rep Med. 2020;1(4):100059.
591 22. Bradley BT, Maioli H, Johnston R, Chaudhry I, Fink SL, Xu H, et al. Histopathology
592 and ultrastructural findings of fatal COVID-19 infections in Washington State: a case series.
593 Lancet. 2020;396(10247):320-32.
594 23. Deshmukh V, Motwani R, Kumar A, Kumari C, Raza K. Histopathological
595 observations in COVID-19: a systematic review. J Clin Pathol. 2020.
596 24. Polak SB, Van Gool IC, Cohen D, von der Thusen JH, van Paassen J. A systematic
597 review of pathological findings in COVID-19: a pathophysiological timeline and possible
598 mechanisms of disease progression. Mod Pathol. 2020;33(11):2128-38.
599 25. Li W, Moore MJ, Vasilieva N, Sui J, Wong SK, Berne MA, et al. Angiotensin-
600 converting enzyme 2 is a functional receptor for the SARS coronavirus. Nature.
601 2003;426(6965):450-4.
602 26. Hoffmann M, Kleine-Weber H, Schroeder S, Kruger N, Herrler T, Erichsen S, et al.
603 SARS-CoV-2 Cell Entry Depends on ACE2 and TMPRSS2 and Is Blocked by a Clinically
604 Proven Protease Inhibitor. Cell. 2020;181(2):271-80 e8.
605 27. Ziegler CGK, Allon SJ, Nyquist SK, Mbano IM, Miao VN, Tzouanas CN, et al.
606 SARS-CoV-2 Receptor ACE2 Is an Interferon-Stimulated Gene in Human Airway Epithelial
607 Cells and Is Detected in Specific Cell Subsets across Tissues. Cell. 2020;181(5):1016-35 e19.
608 28. Trypsteen W, Van Cleemput J, Snippenberg WV, Gerlo S, Vandekerckhove L. On the
609 whereabouts of SARS-CoV-2 in the human body: A systematic review. PLoS Pathog.
610 2020;16(10):e1009037.
611 29. Zaeck LM, Scheibner D, Sehl J, Müller M, Hoffmann D, Beer M, et al. 3D
612 reconstruction of 1 SARS-CoV-2 infection in ferrets emphasizes focal infection pattern in the
613 upper respiratory tract. 2020.
614 30. Triana S, Metz Zumaran C, Ramirez C, Kee C, Doldan P, Shahraz M, et al. Single-
615 cell analyses reveal SARS-CoV-2 interference with intrinsic immune response in the human
616 gut. bioRxiv. 2020:2020.10.21.348854.
617 31. Stanifer ML, Kee C, Cortese M, Zumaran CM, Triana S, Mukenhirn M, et al. Critical
618 Role of Type III Interferon in Controlling SARS-CoV-2 Infection in Human Intestinal
619 Epithelial Cells. Cell Rep. 2020;32(1):107863.
620 32. Youk J, Kim T, Evans KV, Jeong YI, Hur Y, Hong SP, et al. Three-Dimensional
621 Human Alveolar Stem Cell Culture Models Reveal Infection Response to SARS-CoV-2. Cell
622 Stem Cell. 2020.
623 33. Moein S, Javanmard SH, Abedi M, Izadpanahi MH, Gheisari Y. Identification of
624 Appropriate Housekeeping Genes for Gene Expression Analysis in Long-term Hypoxia-
625 treated Kidney Cells. Adv Biomed Res. 2017;6:15.
626 34. Curina A, Termanini A, Barozzi I, Prosperini E, Simonatto M, Polletti S, et al. High
627 constitutive activity of a broad panel of housekeeping and tissue-specific cis-regulatory
628 elements depends on a subset of ETS proteins. Genes Dev. 2017;31(4):399-412.
629 35. Eisenberg E, Levanon EY. Human housekeeping genes, revisited. Trends Genet.
630 2013;29(10):569-74.
631 36. Desmyter J, Melnick JL, Rawls WE. Defectiveness of interferon production and of
632 rubella virus interference in a line of African green monkey kidney cells (Vero). J Virol.
633 1968;2(10):955-61.

634 37. Mosca JD, Pitha PM. Transcriptional and posttranscriptional regulation of exogenous
635 human beta interferon gene in simian cells defective in interferon synthesis. Mol Cell Biol.
636 1986;6(6):2279-83.
637 38. Felgenhauer U, Schoen A, Gad HH, Hartmann R, Schaubmar AR, Failing K, et al.
638 Inhibition of SARS-CoV-2 by type I and type III interferons. J Biol Chem.
639 2020;295(41):13958-64.
640 39. Milewska A, Kula-Pacurar A, Wadas J, Suder A, Szczepanski A, Dabrowska A, et al.
641 Replication of Severe Acute Respiratory Syndrome Coronavirus 2 in Human Respiratory
642 Epithelium. J Virol. 2020;94(15).
643 40. Sia SF, Yan LM, Chin AWH, Fung K, Choy KT, Wong AYL, et al. Pathogenesis and
644 transmission of SARS-CoV-2 in golden hamsters. Nature. 2020;583(7818):834-8.
645 41. Kim YI, Kim SG, Kim SM, Kim EH, Park SJ, Yu KM, et al. Infection and Rapid
646 Transmission of SARS-CoV-2 in Ferrets. Cell Host Microbe. 2020;27(5):704-9 e2.
647 42. Hassan AO, Case JB, Winkler ES, Thackray LB, Kafai NM, Bailey AL, et al. A
648 SARS-CoV-2 Infection Model in Mice Demonstrates Protection by Neutralizing Antibodies.
649 Cell. 2020;182(3):744-53 e4.
650 43. Muralidharan S, Mandrekar P. Cellular stress response and innate immune signaling:
651 integrating pathways in host defense and inflammation. J Leukoc Biol. 2013;94(6):1167-84.
652 44. Hadjadj J, Yatim N, Barnabei L, Corneau A, Boussier J, Smith N, et al. Impaired type
653 I interferon activity and inflammatory responses in severe COVID-19 patients. Science.
654 2020;369(6504):718-24.
655 45. Hao S, Ning K, Kuz CA, Vorhies K, Yan Z, Qiu J. Long-Term Modeling of SARS-
656 CoV-2 Infection of In Vitro Cultured Polarized Human Airway Epithelium. mBio.
657 2020;11(6).
658 46. Kindler E, Jonsdottir HR, Muth D, Hamming OJ, Hartmann R, Rodriguez R, et al.
659 Efficient replication of the novel human betacoronavirus EMC on primary human epithelium
660 highlights its zoonotic potential. mBio. 2013;4(1):e00611-12.
661 47. Oyler-Yaniv A, Oyler-Yaniv J, Whitlock BM, Liu Z, Germain RN, Huse M, et al. A
662 Tunable Diffusion-Consumption Mechanism of Cytokine Propagation Enables Plasticity in
663 Cell-to-Cell Communication in the Immune System. Immunity. 2017;46(4):609-20.
664 48. Oyler-Yaniv J, Oyler-Yaniv A, Shakiba M, Min NK, Chen YH, Cheng SY, et al.
665 Catch and Release of Cytokines Mediated by Tumor Phosphatidylserine Converts Transient
666 Exposure into Long-Lived Inflammation. Mol Cell. 2017;66(5):635-47 e7.
667 49. Tapia K, Kim WK, Sun Y, Mercado-Lopez X, Dunay E, Wise M, et al. Defective
668 viral genomes arising in vivo provide critical danger signals for the triggering of lung
669 antiviral immunity. PLoS Pathog. 2013;9(10):e1003703.
670 50. Killip MJ, Jackson D, Perez-Cidoncha M, Fodor E, Randall RE. Single-cell studies of
671 IFN-beta promoter activation by wild-type and NS1-defective influenza A viruses. J Gen
672 Virol. 2017;98(3):357-63.
673 51. Vasilijevic J, Zamarreno N, Oliveros JC, Rodriguez-Frandsen A, Gomez G,
674 Rodriguez G, et al. Reduced accumulation of defective viral genomes contributes to severe
675 outcome in influenza virus infected patients. PLoS Pathog. 2017;13(10):e1006650.
676 52. Russell AB, Elshina E, Kowalsky JR, Te Velthuis AJW, Bloom JD. Single-Cell Virus
677 Sequencing of Influenza Infections That Trigger Innate Immunity. J Virol. 2019;93(14).
678 53. Li G, Zhang J, Tong X, Liu W, Ye X. Heat shock protein 70 inhibits the activity of
679 Influenza A virus ribonucleoprotein and blocks the replication of virus in vitro and in vivo.
680 PLoS One. 2011;6(2):e16546.
681 54. Hirayama E, Atagi H, Hiraki A, Kim J. Heat shock protein 70 is related to thermal
682 inhibition of nuclear export of the influenza virus ribonucleoprotein complex. J Virol.
683 2004;78(3):1263-70.

684 55. Wan Q, Song D, Li H, He ML. Stress proteins: the biological functions in virus
685 infection, present and challenges for target-based antiviral drug development. Signal
686 Transduct Target Ther. 2020;5(1):125.
687 56. Plante JA, Plante KS, Gralinski LE, Beall A, Ferris MT, Bottomly D, et al. Mucin 4
688 Protects Female Mice from Coronavirus Pathogenesis. bioRxiv. 2020:2020.02.19.957118.
689 57. Ehre C, Worthington EN, Liesman RM, Grubb BR, Barbier D, O'Neal WK, et al.
690 Overexpressing mouse model demonstrates the protective role of Muc5ac in the lungs. Proc
691 Natl Acad Sci U S A. 2012;109(41):16528-33.
692 58. Wang P, Xu J, Wang Y, Cao X. An interferon-independent lncRNA promotes viral
693 replication by modulating cellular metabolism. Science. 2017;358(6366):1051-5.
694 59. Dalton RM, Mullin AE, Amorim MJ, Medcalf E, Tiley LS, Digard P. Temperature
695 sensitive influenza A virus genome replication results from low thermal stability of
696 polymerase-cRNA complexes. Virol J. 2006;3:58.
697 60. Long JS, Mistry B, Haslam SM, Barclay WS. Host and viral determinants of
698 influenza A virus species specificity. Nat Rev Microbiol. 2019;17(2):67-81.
699 61. Deng X, Mettelman RC, O'Brien A, Thompson JA, E. T, O'Brien TE, et al. Analysis
700 of Coronavirus Temperature-Sensitive Mutants Reveals an Interplay between the
701 Macrodomain and Papain-Like Protease Impacting Replication and Pathogenesis. Journal of
702 Virology. 2019;93(12):e021140-18.
703 62. Hierholzer JC, Killington RA. 2 - Virus isolation and quantitation. In: Mahy BWJ,
704 Kangro HO, editors. Virology Methods Manual. London: Academic Press; 1996. p. 25-46.
705 63. Flohr F, Schneider-Schaulies S, Haller O, Kochs G. The central interactive region of
706 human MxA GTPase is involved in GTPase activation and interaction with viral target
707 structures. FEBS Lett. 1999;463(1-2):24-8.
708 64. Kim D, Langmead B, Salzberg SL. HISAT: a fast spliced aligner with low memory
709 requirements. Nat Methods. 2015;12(4):357-60.
710 65. Langmead B, Salzberg SL. Fast gapped-read alignment with Bowtie 2. Nat Methods.
711 2012;9(4):357-9.
712 66. Liao Y, Smyth GK, Shi W. featureCounts: an efficient general purpose program for
713 assigning sequence reads to genomic features. Bioinformatics. 2014;30(7):923-30.
714 67. Robinson MD, McCarthy DJ, Smyth GK. edgeR: a Bioconductor package for
715 differential expression analysis of digital gene expression data. Bioinformatics.
716 2010;26(1):139-40.
717 68. Fabregat A, Jupe S, Matthews L, Sidiropoulos K, Gillespie M, Garapati P, et al. The
718 Reactome Pathway Knowledgebase. Nucleic Acids Res. 2018;46(D1):D649-D55.
719 69. Jassal B, Matthews L, Viteri G, Gong C, Lorente P, Fabregat A, et al. The reactome
720 pathway knowledgebase. Nucleic Acids Res. 2020;48(D1):D498-D503.
721 70. Zhou Y, Zhou B, Pache L, Chang M, Khodabakhshi AH, Tanaseichuk O, et al.
722 Metascape provides a biologist-oriented resource for the analysis of systems-level datasets.
723 Nat Commun. 2019;10(1):1523.
724

725

Figure legends

Figure 1. Differentiation of primary bronchial epithelial airway cultures supports SARS-CoV-2 replication. Primary bronchiole epithelial cells were seeded onto 6.5mm transwells and grown to confluency prior to differentiation under air liquid interface (ALI) conditions for ≥35 days. Ciliated respiratory cultures were mock (media only) or SARS-CoV-2 (SCV2; 10^4 PFU/well) infected at 37°C for the indicated times (hours, h). (A) Representative images of H&E (left-hand panels), ACE2 (brown, middle panels), or detection of SCV2 RNA by *in situ* hybridization (red, right-hand panels) stained sections. Haematoxylin was used as a counter stain. Scale bars = 20 μm. (B/C) Genome copies per ml of SCV2 in apical washes harvested over time as determined RT-qPCR. N≥7 derived from a minimum of three independent biological experiments per sample condition. (B) Black line, median; all data points shown. (C) Means and SD shown. (D) Specificity of RT-qPCR to detect vRNA in apical washes taken from mock (blue circles) or SCV2 infected (red circles) tissues at 72 h (as in B). N≥5 derived from a minimum of three independent biological experiments per sample condition. Black line, median; all data points shown; p=0.0003, Mann-Whitney *U*-test. (E) $TCID_{50}$ assay measuring infectious viral load in apical washes harvested from mock (blue circles) or SCV2 infected (red circles) tissues over time. Means and SD shown. N≥5 derived from a minimum of three independent biological experiments per sample condition.

Figure 2. SARS-CoV-2 infection of respiratory airway cultures induces a type-I and type-III IFN response. Ciliated respiratory cultures were mock (media only) or SARS-CoV-2 (SCV2; 10^4 PFU/well) infected at 37°C for 72 h prior to RNA extraction and RNA-Seq. (A) Scatter plots showing high confidence ($p<0.05$) differentially expressed gene (DEG) transcripts identified between mock and SCV2 infected cultures (grey circles); DEGs ≥ 1.5

log2 FC, red circles; DEGs ≤ -1.5 log2 FC, blue circles. (B) Reactome pathway analysis of mapped DEGs ($p<0.05$, ≥ 1.5 log2 FC). Pathways enriched for DEGs with an FDR (corrected over-representation *P* value) < 0.05 (plotted as -log10 FDR) shown (red bars). Dotted line, threshold of significance (-log10 FDR of 0.05). (C) Expression profile (log2 CPM) of Immune system (R-HSA168256) related DEGs (identified in B). Black line, median; dotted lines; 5th and 95th percentile range; $p<0.0001$, Mann-Whitney *U*-test. (D) Expression levels (log2 CPM) of individual Immune system DEGs (identified in B); $p<0.0001$, Wilcoxon matched-pairs sign rank test. (A to D) RNA-Seq data derived from RNA isolated from three technical replicates per sample condition. Data analysis is presented in Supplemental File S1. (E) Indirect immunofluorescence staining of tissue sections showing Mx1 (green) and SCV2 nucleocapsid (N, red) epithelial localization. Nuclei were stained with DAPI. Scale bars = 20 µm.

Figure 3. Respiratory airway cultures induce a heat stress response upon incubation at elevated temperature. Ciliated respiratory cultures were incubated at 37, 39, or 40°C for 72 h prior to fixation or RNA extraction and RNA-Seq. (A) Representative images of H&E stained sections. Scale bars = 20 µm. (B) Quantitation of respiratory tissue thickness (µm) at 72 h. N=300 measurements derived from three technical replicates per sample condition. Black line, median; dotted lines; 5th and 95th percentile range; p-values shown, one-way ANOVA Kruskal-Wallis test. (C) ACE2 expression levels (CPM) in respiratory cultures incubated at 37 or 40°C; means and SD shown; $p=0.4001$, Mann-Whitney *U*-test. (D) Expression values (log2 CPM) of a reference gene set (24 genes; (33-35)) in respiratory cultures incubated at 37 or 40°C; $p=0.9106$, Mann-Whitney *U*-test. (E) Scatter plots showing high confidence ($p<0.05$) differentially expressed gene (DEG) transcripts identified between respiratory cultures incubated at 37 or 40°C (grey circles); DEGs ≥ 1.5 log2 FC, red circles;

776 DEGs ≤ -1.5 log2 FC, blue circles. (F) Reactome pathway analysis of mapped DEGs ($p<0.05$,
777 ≥ 1.5 log2 FC). Pathways enriched for DEGs with an FDR < 0.05 (plotted as -log10 FDR)
778 shown (red bars; every 4th bar labelled). Dotted line, threshold of significance (-log10 FDR of
779 0.05). (G) Expression values (log2 CPM) of DEGs identified with cellular response to heat
780 stress (R-HSA-3371556; arrow in B) and cellular response to external stimuli (R-HSA-
781 8953897) pathways; p=0.001, Wilcoxon matched-pairs sign ranked test. (H) Expression
782 levels (log2 CPM) for all genes associated with cellular response to heat stress pathway (R-
783 HSA-3371556); p=0.0013, Wilcoxon matched-pairs sign ranked test. (C to H) RNA-Seq data
784 derived from RNA isolated from three technical replicates per sample condition. Data
785 analysis is presented in Supplemental File S2.
786
787 **Figure 4. Elevated temperature restricts SARS-CoV-2 replication in respiratory airway**
788 **cultures.** Ciliated respiratory cultures were incubated at 37, 39, or 40°C for 24 h prior to
789 mock (media only) or SARS-CoV-2 (SCV2; 10^4 PFU/well) infection and incubation at the
790 indicated temperatures. Apical washes were collected over time (as indicated) and tissues
791 harvested at 72 h for RNA extraction and RNA-Seq. (A/B) Genome copies per ml of SCV2
792 in apical washes harvested over time as determined RT-qPCR. N≥11 derived from a
793 minimum of three independent biological experiments per sample condition. (A) Means and
794 SD shown. (B) Black line, median; whisker, 95% confidence interval; all data points shown;
795 p-values shown, one-way ANOVA Kruskal-Wallis test. (C/D) $TCID_{50}$ assay measuring
796 infectious viral load in apical washes harvested from SCV2 infected respiratory cultures over
797 time. N≥11 derived from a minimum of three independent biological experiments. (C) Means
798 and SD shown. (D) Black line, median; whisker, 95% confidence interval; all data points
799 shown; p-values shown, one-way ANOVA Kruskal-Wallis test. (E) Genome copies per tissue
800 of SCV2 as determined RT-qPCR. N≥11 derived from a minimum of three independent

biological experiments per sample condition. Black line, median; whisker, 95% confidence interval; all data points shown; p-values shown, one-way ANOVA Kruskal-Wallis test.

Figure 5. Respiratory airway cultures induce distinct transcriptional host responses to SARS-CoV-2 infection at elevated temperature. Ciliated respiratory cultures were incubated at 37 or 40°C for 24 h prior to mock (media only) or SARS-CoV-2 (SCV2; 10^4 PFU/well) infection. Tissue were incubated at their respective temperatures for 72 h prior to RNA extraction and RNA-Seq. DEGs ($p<0.05$, ≥ 1.5 log2 FC [top panels] or ≤ -1.5 log2 FC [bottom panels]) were identified for each paired condition; blue ellipses, SCV2 37°C/Mock 37°C (SCV37/Mock37); green ellipses, SCV2 40°C/Mock 40°C (SCV40/Mock40); red ellipses, SCV2 40°C/Mock 37°C (SCV40/Mock37); yellow ellipses, Mock 40°C/Mock 37°C (Mock40/Mock37). (A) Venn diagram showing the number of unique or shared DEGs between each paired condition analyzed. (B) Circos plot showing the proportion of unique (light orange inner circle) or shared (dark orange inner circle + purple lines) DEGs between each paired condition analyzed. Blue lines, DEGs which share pathway gene ontology terms. (C) Metascape pathway analysis showing DEG enrichment p-value (-log10) for each paired condition analyzed. Grey boxes, $p>0.05$. (A to C) RNA-Seq data derived from RNA isolated from three technical replicates per sample condition. Data analysis is presented in Supplemental Files S1 to S5.

Figure 6. Elevated temperature restricts SARS-CoV-2 replication in respiratory airway cultures independently of the induction of IFN-mediated innate immune defences. Ciliated respiratory cultures were incubated at 37 or 40°C for 24h prior to mock (media) or SARS-CoV-2 (SCV2; 10^4 PFU/well) infection. Tissue were incubated at their respective temperatures for 72 h prior to RNA extraction and RNA-Seq. (A) Scatter plots showing high

826 confidence ($p<0.05$) differentially expressed gene (DEG) transcripts identified between 37
827 and 40°C SCV2 infected respiratory cultures (grey circles); DEGs ≥ 1.5 log2 FC, red circles;
828 DEGs ≤ -1.5 log2 FC, blue circles. (B) Reactome pathway analysis of mapped DEGs
829 ($p<0.05$, ≤ -1.5 log2 FC). Pathways enriched for DEGs with an FDR< 0.05 (plotted as -log10
830 FDR) shown (blue bars). Dotted line, threshold of significance (-log10 FDR of 0.05). (C)
831 Expression profile (log2 CPM) of Immune system (R-HSA168256) DEGs (identified in B)
832 relative to expression levels in Mock tissue incubated at 37 and 40°C. Black line, median;
833 dotted lines, 5th and 95th percentile range; p-values shown, Wilcoxon matched-pairs signed
834 rank test (top), one-way ANOVA Friedman test (bottom). (D) Expression levels (log2 CPM)
835 for individual Immune system (R-HAS-168256) DEGs (identified in B) relative to mock at
836 37 and 40°C. (A to D) RNA-Seq data derived from RNA isolated from three technical
837 replicates per sample condition. Data analysis is presented in Supplemental File S7.
838
839 **Figure 7. Elevated temperature restricts SARS-CoV-2 replication in VeroE6 cells.**
840 Permissive VeroE6 cells were infected with SARS-CoV-2 (SCV2; 10^4 PFU/well) at 37°C
841 prior to temperature elevation and incubation at 37, 39, or 40°C (A/B) or pre-incubated at 37,
842 39, or 40°C for 24 h prior to infection and continued incubation at their respective
843 temperatures (C). (A) $TCID_{50}$ growth curve of SCV2 infected VeroE6 cells incubated at 37°C
844 over time (h). Means and SD shown. (B/C) $TCID_{50}$ viral titres at 24 and 48 h post-infection.
845 Left-hand panel; means and SD. Right-hand panel; black line, median; whisker, 95%
846 confidence interval; all data points shown; p-values shown, one-way ANOVA Kruskal-
847 Wallis test. (A-C) N=9 derived from a minimum of three independent biological experiments
848 per sample condition. (D) Expression profile (log2 CPM) for genes associated with cellular
849 response to heat (GO:0034605) in respiratory cultures (Resp. tissue), undifferentiated
850 primary HBE, and VeroE6 cells incubated at 37°C; p-values shown, One-way ANOVA

Friedman test. (E) Expression levels (log2 CPM) of individual genes associated with cellular response to heat (as in D). (F) Expression profile (log2 CPM) of a reference gene set (18 genes; (33-35)); p-values shown, One-way ANOVA Friedman test. (G) Expression values (log2 CPM) of a reference gene set (as in F). (D to G) RNA-Seq data derived from RNA isolated from three technical replicates per sample condition. Data analysis is presented in Supplemental File S8.

Figure 8. Elevated temperature restricts SARS-CoV-2 transcription in respiratory airway cultures. Ciliated respiratory cultures were incubated at 37 or 40°C for 24 h prior to mock (media only) or SARS-CoV-2 (SCV2; 10^4 PFU/well) infection. Tissue were incubated at their respective temperatures for 72 h prior to RNA extraction and RNA-Seq. (A) Total mapped reads (MR; human + SCV2) from infected tissues; means and SD shown; p=0.3429, one-way ANOVA Kruskal-Wallis test. (B) SCV2 mapped reads from infected tissues; means and SD shown. (C) % SCV2 mapped reads of total mapped read count (human + SCV2); means and SD shown. (D) Expression values (log2 MR) of SCV2 gene transcripts; p<0.0010, Wilcoxon matched-pairs sign rank test. (A-D) RNA-Seq data derived from RNA isolated from three technical replicates per sample condition. (E) Indirect immunofluorescence staining of tissue sections showing SCV2 nucleocapsid (N, red) epithelial localization. Nuclei were stained with DAPI. Scale bars = 20 µm. (F) Quantitation of SCV2 N infectious foci in respiratory tissue sections. N=6 independently stained tissue sections per sample condition. Black line, median; whisker, 95% confidence interval; all data points shown; p=0.0022, Mann-Whitney *U*-test.

Figure S1. Respiratory airway cultures induce a heat stress response. Ciliated respiratory cultures were incubated at 37 or 40°C for 72 h prior to RNA extraction and RNA-Seq. Heat

map showing expression values (log2 CPM) of genes associated with the cellular response to heat pathway (GO: 0034605); p=0.0018, Wilcoxon matched-pairs sign rank test; every second row labelled. RNA-Seq data derived from RNA isolated from three technical replicates per sample condition. Data analysis is presented in Supplemental File S2.

Figure S2. Identification of DEGs in mock and SARS-CoV-2 infected respiratory cultures incubated at 40°C. Ciliated respiratory cultures were incubated at 40°C for 24 h prior to mock (media only) or SARS-CoV-2 (SCV2; 10^4 PFU/well) infection and continued incubation at 40°C. Tissues were harvested at 72 h for RNA extraction and RNA-Seq. (A) Scatter plots showing high confidence ($p<0.05$) differentially expressed gene (DEG) transcripts identified between mock and SCV2 infected respiratory cultures at 40°C (grey circles); DEGs ≥ 1.5 log2 FC, red circles; DEGs ≤ -1.5 log2 FC, blue circles. (B) Reactome pathway analysis of mapped DEGs ($p<0.05$, ≥ 1.5 log2 FC [red bars] or ≤ -1.5 log2 FC [blue bars]). Top 10 enriched pathways shown. Dotted line, threshold of significance (-log10 FDR of 0.05). (C) Expression values (log2 CPM) of Reactome mapped DEGs; p-values shown, Wilcoxon matched-pairs sign rank test. (A to C) RNA-Seq data derived from RNA isolated from three technical replicates per sample condition. Data analysis is presented in Supplemental File S3.

Figure S3. Identification of DEGs in mock and SARS-CoV-2 infected respiratory cultures incubated at 37 and 40°C, respectively. Ciliated respiratory cultures were incubated at 37 or 40°C for 24 h prior to mock (media only) or SARS-CoV-2 (SCV2; 10^4 PFU/well) infection and continued incubation at their respective temperatures. Tissues were harvested at 72 h for RNA extraction and RNA-Seq. (A) Scatter plots showing high

confidence ($p<0.05$) differentially expressed gene (DEG) transcripts identified between mock (37°C) and SCV2 infected (40°C) respiratory cultures (grey circles); DEGs ≥ 1.5 log2 FC, red circles; DEGs ≤ -1.5 log2 FC, blue circles. (B) Reactome pathway analysis of mapped DEGs ($p<0.05$, ≥ 1.5 log2 FC [red bars, every sixth row labelled] or ≤ -1.5 log2 FC [blue bars]). Dotted line, threshold of significance (-log10 FDR of 0.05). Black arrow, identification of cellular response to heat stress pathway. (C) Expression values (log2 CPM) of Reactome mapped DEGs; p-values shown, Wilcoxon matched-pairs sign rank test. Every third column labelled. (A to C) RNA-Seq data derived from RNA isolated from three technical replicates per sample condition. Data analysis is presented in Supplemental File S4.

Figure S4. Respiratory airway cultures induce distinct lncRNA and miRNA transcriptional host responses to SARS-CoV-2 infection at elevated temperature. Ciliated respiratory cultures were incubated at 37 or 40°C for 24 h prior to mock (media only) or SARS-CoV-2 (SCV2; 10^4 PFU/well) infection. Tissue were incubated at their respective temperatures for 72 h prior to RNA extraction and RNA-Seq. DEGs ($p<0.05$, ≥ 1.5 log2 FC [top panels] or ≤ -1.5 log2 FC [bottom panels]) were identified for each paired condition; blue circles/ellipses, SCV2 37°C/Mock 37°C (SCV37/Mock37); green circles/ellipses, SCV2 40°C/Mock 40°C (SCV40/Mock40); red circles/ellipses, SCV2 40°C/Mock 37°C (SCV40/Mock37); yellow circles/ellipses, Mock 40°C/Mock 37°C (Mock40/Mock37). (A) Proportion of lncRNA + miRNA (grey numbers and lines [relative %]) identified per DEG population (coloured numbers and lines [relative %]). (B) Venn diagram showing the number of unique or shared lncRNA + miRNAs identified between each paired condition analyzed. (C) Circos plot showing the proportion of unique (light orange inner circle) or shared (dark orange inner circle + purple lines) lncRNA + miRNAs between each paired condition analyzed. (D) Expression values (log2 CPM) of lncRNA +

926 miRNA identified per sample condition analyzed; p-values shown, one-way ANOVA
927 Friedman test (top), Wilcoxon matched-pairs sign rank test (bottom). (A to D) RNA-Seq data
928 derived from RNA isolated from three technical replicates per sample condition. Data
929 analysis is presented in Supplemental File S6.
930

931 ## Supplementary Files

932 **Supplemental File S1.** RNA-Seq data analysis for mock (Mck)-treated or SARS-CoV-2
933 (SCV2) infected respiratory tissues at 37°C.
934 **Supplemental File S2.** RNA-Seq data analysis for mock (Mck)-treated respiratory tissues
935 incubated at 37 and 40°C.
936 **Supplemental File S3.** RNA-Seq data analysis for mock (Mck)-treated or SARS-CoV-2
937 (SCV2) infected respiratory tissues at 40°C.
938 **Supplemental File S4.** RNA-Seq data analysis for mock (Mck)-treated or SARS-CoV-2
939 (SCV2) infected respiratory tissues at 37°C and 40°C, respectively.
940 **Supplemental File S5.** Comparative DEG analysis of RNA-Seq data derived from mock
941 (Mck)-treated or SARS-CoV-2 (SCV2) infected respiratory tissues at 37 and 40°C.
942 Supplemental Files S1-S4.
943 **Supplemental File S6.** Comparative lncRNA and miRNA DEG analysis of RNA-Seq data
944 derived from mock (Mck)-treated or SARS-CoV-2 (SCV2) infected respiratory tissues at 37
945 and 40°C. Supplemental Files S1-S4.
946 **Supplemental File S7.** RNA-Seq data analysis for SARS-CoV-2 (SCV2) infected respiratory
947 tissues at 37 and 40°C.
948 **Supplemental File S8.** DEG analysis of the Cellular response to heat (GO:0034605) from
949 RNA-Seq data derived from mock (Mck)-treated respiratory tissues (Resp. tissue) and
950 undifferentiated HBEC and VeroE6 cells incubated at 37°C.

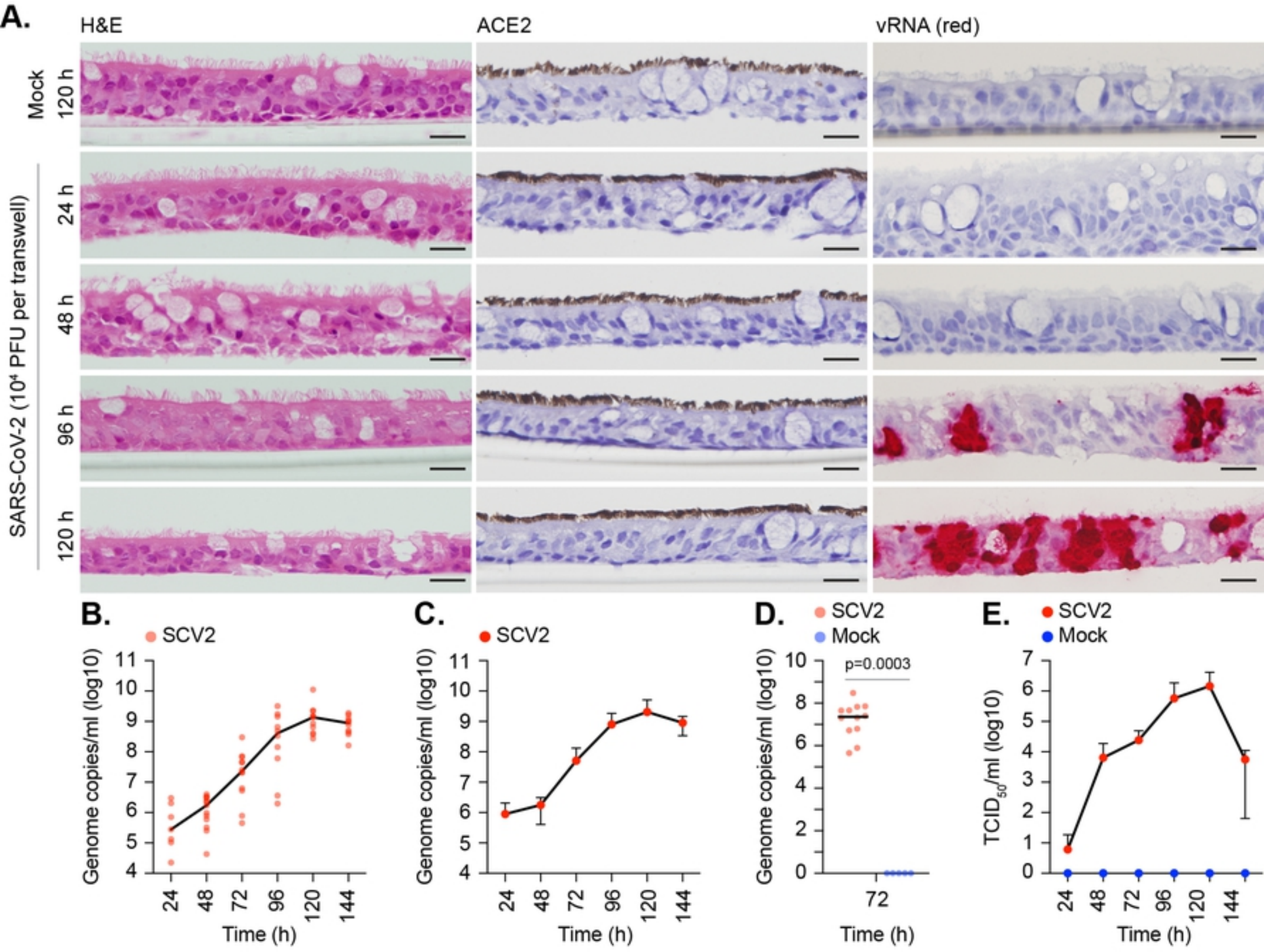
A.
H&E
ACE2
vRNA (red)
Mock
120 h
SARS-CoV-2 (10^4 PFU per transwell)
24 h
48 h
96 h
120 h
B.
SCV2
Genome copies/ml (log10)
Time (h)
C.
SCV2
Genome copies/ml (log10)
Time (h)
D.
SCV2
Mock
p=0.0003
Genome copies/ml (log10)
Time (h)
E.
SCV2
Mock
$TCID_{50}$/ml (log10)
Time (h)

Fig 1

A.

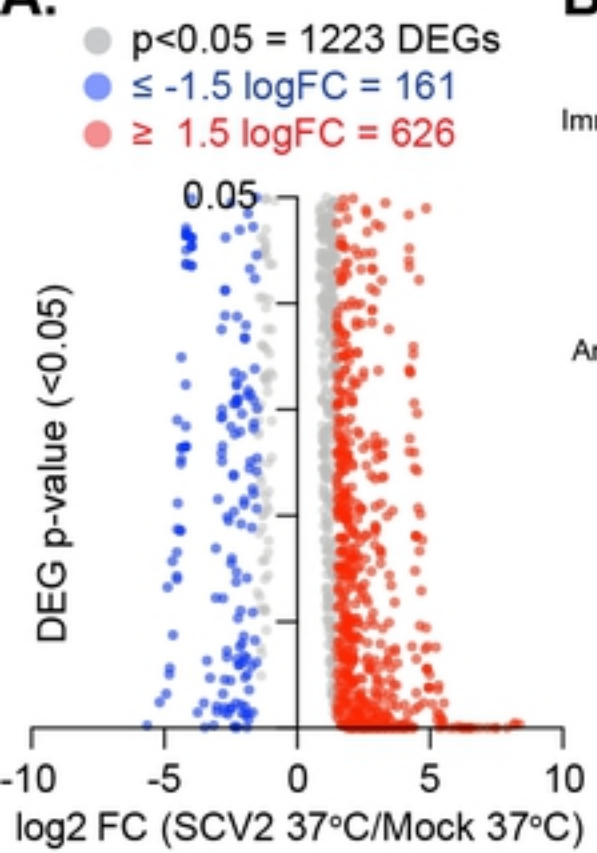
p<0.05 = 1223 DEGs
≤ -1.5 logFC = 161
≥ 1.5 logFC = 626
0.05
DEG p-value (<0.05)
-10
-5
0
5
10
log2 FC (SCV2 37°C/Mock 37°C)

B.

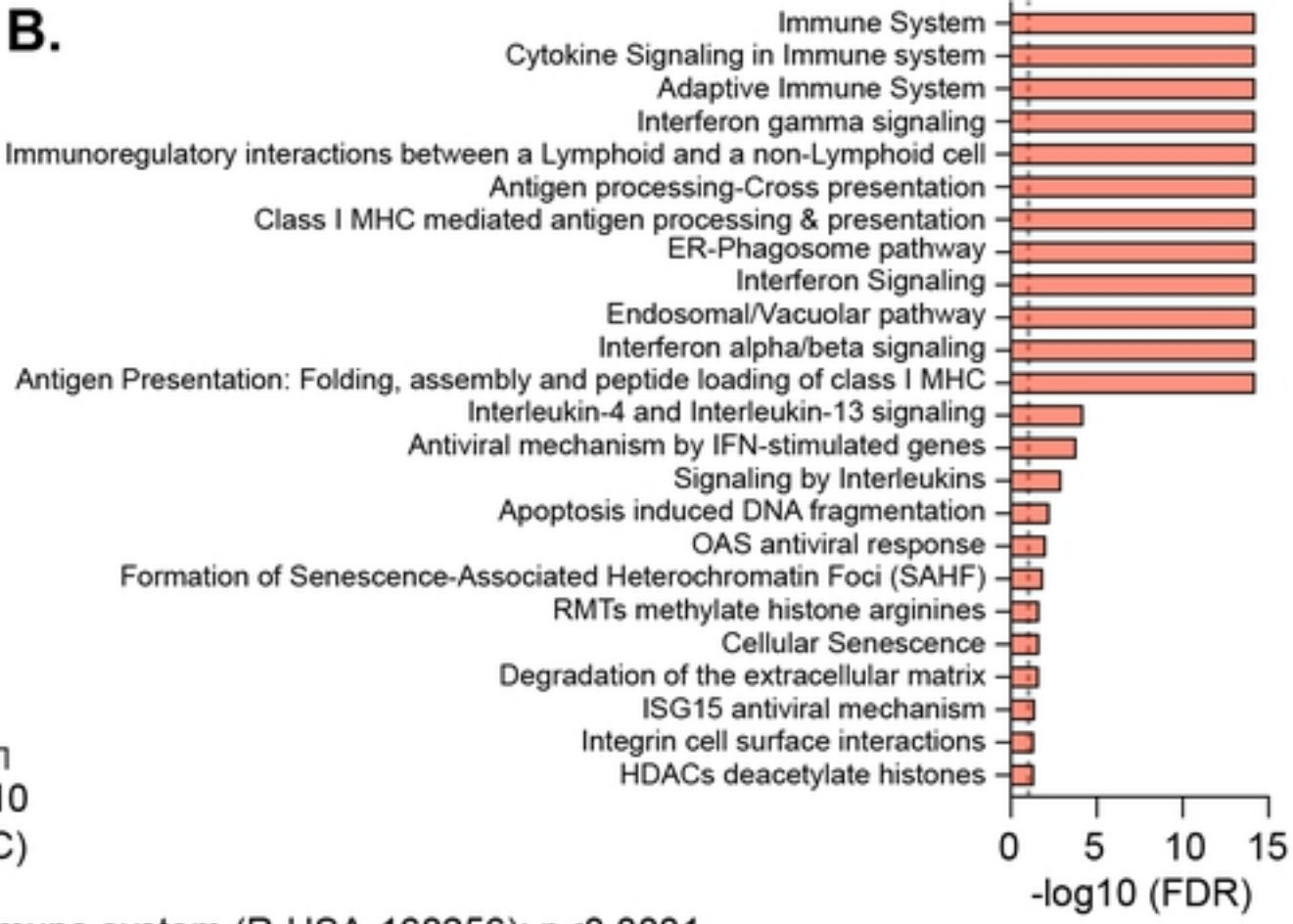
Immune System
Cytokine Signaling in Immune system
Adaptive Immune System
Interferon gamma signaling
Immunoregulatory interactions between a Lymphoid and a non-Lymphoid cell
Antigen processing-Cross presentation
Class I MHC mediated antigen processing & presentation
ER-Phagosome pathway
Interferon Signaling
Endosomal/Vacuolar pathway
Interferon alpha/beta signaling
Antigen Presentation: Folding, assembly and peptide loading of class I MHC
Interleukin-4 and Interleukin-13 signaling
Antiviral mechanism by IFN-stimulated genes
Signaling by Interleukins
Apoptosis induced DNA fragmentation
OAS antiviral response
Formation of Senescence-Associated Heterochromatin Foci (SAHF)
RMTs methylate histone arginines
Cellular Senescence
Degradation of the extracellular matrix
ISG15 antiviral mechanism
Integrin cell surface interactions
HDACs deacetylate histones
0
5
10
15
-log10 (FDR)

C.

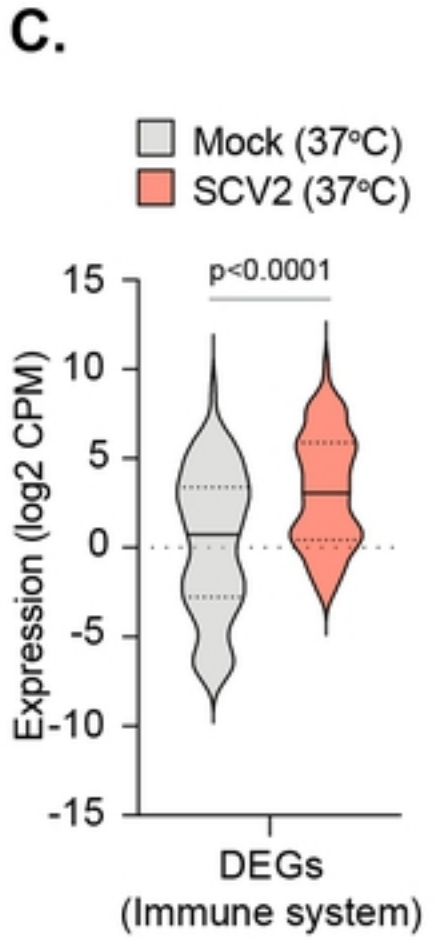
Mock (37°C)
SCV2 (37°C)
p<0.0001
15
10
5
0
-5
-10
-15
Expression (log2 CPM)
DEGs
(Immune system)

D.

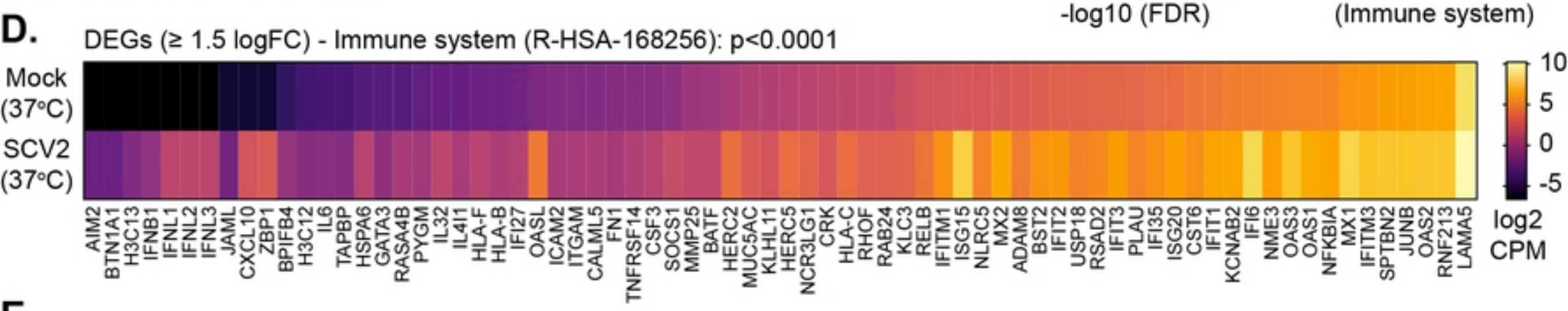
DEGs (≥ 1.5 logFC) - Immune system (R-HSA-168256): p<0.0001
Mock (37°C)
SCV2 (37°C)
10
5
0
-5
log2 CPM
AIM2
BTN1A1
H3C13
IFNB1
IFNL1
IFNL2
IFNL3
JAML
CXCL10
ZBP1
BPIFB4
H3C12
IL6
TAPBP
HSPA6
GATA3
RASA4B
PYGM
IL32
IL4I1
HLA-F
HLA-B
IFI27
OASL
ICAM2
ITGAM
CALML5
FN1
TNFRSF14
CSF3
SOCS1
MMP25
BATF
HERC2
MUC5AC
KLHL11
HERC5
NCR3LG1
CRK
HLA-C
RHOF
RAB24
KLC3
RELB
IFITM1
ISG15
NLRC5
MX2
ADAM8
BST2
IFIT2
USP18
RSAD2
IFIT3
PLAU
IFI35
ISG20
CST6
IFIT1
KCNAB2
IFI6
NME3
OAS3
OAS1
NFKBIA
MX1
IFITM3
SPTBN2
JUNB
OAS2
RNF213
LAMA5

E.

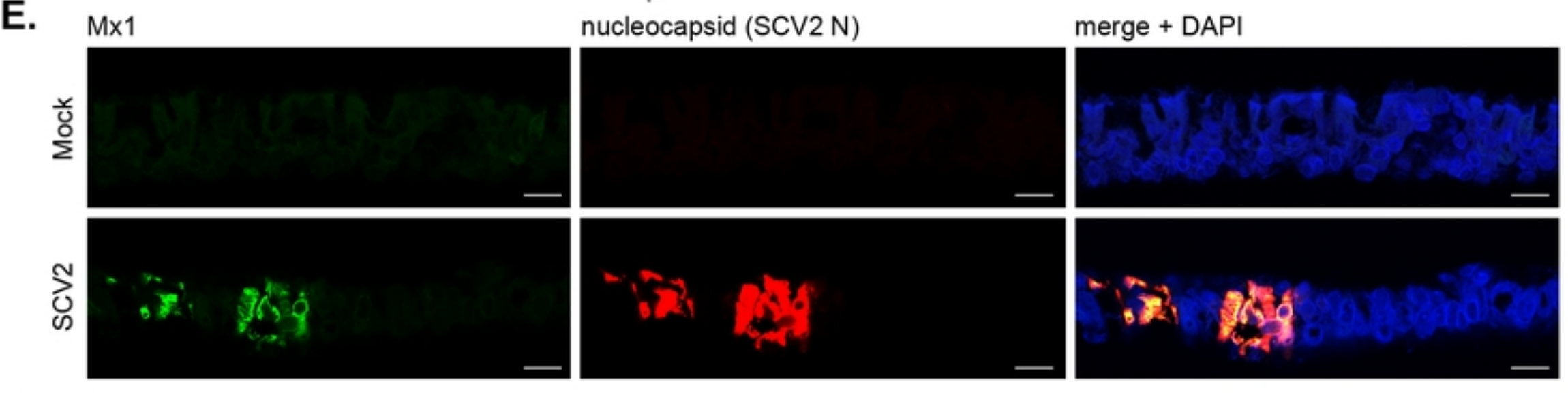
Mx1
nucleocapsid (SCV2 N)
merge + DAPI
Mock
SCV2

Fig 2

Fig 3

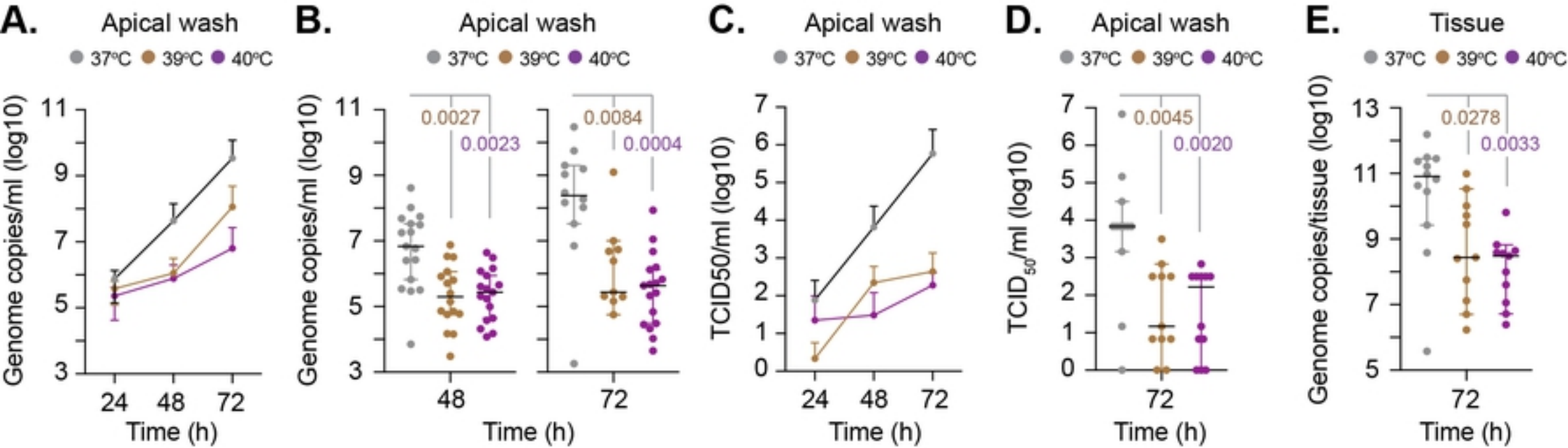
A.
Apical wash
37°C 39°C 40°C
Genome copies/ml (log10)
11
9
7
5
3
24 48 72
Time (h)
B.
Apical wash
37°C 39°C 40°C
Genome copies/ml (log10)
0.0027
0.0023
0.0084
0.0004
48 72
Time (h)
C.
Apical wash
37°C 39°C 40°C
TCID50/ml (log10)
7
6
5
4
3
2
1
0
24 48 72
Time (h)
D.
Apical wash
37°C 39°C 40°C
TCID50/ml (log10)
0.0045
0.0020
72
Time (h)
E.
Tissue
37°C 39°C 40°C
Genome copies/tissue (log10)
13
11
9
7
5
0.0278
0.0033
72
Time (h)

Manuscript

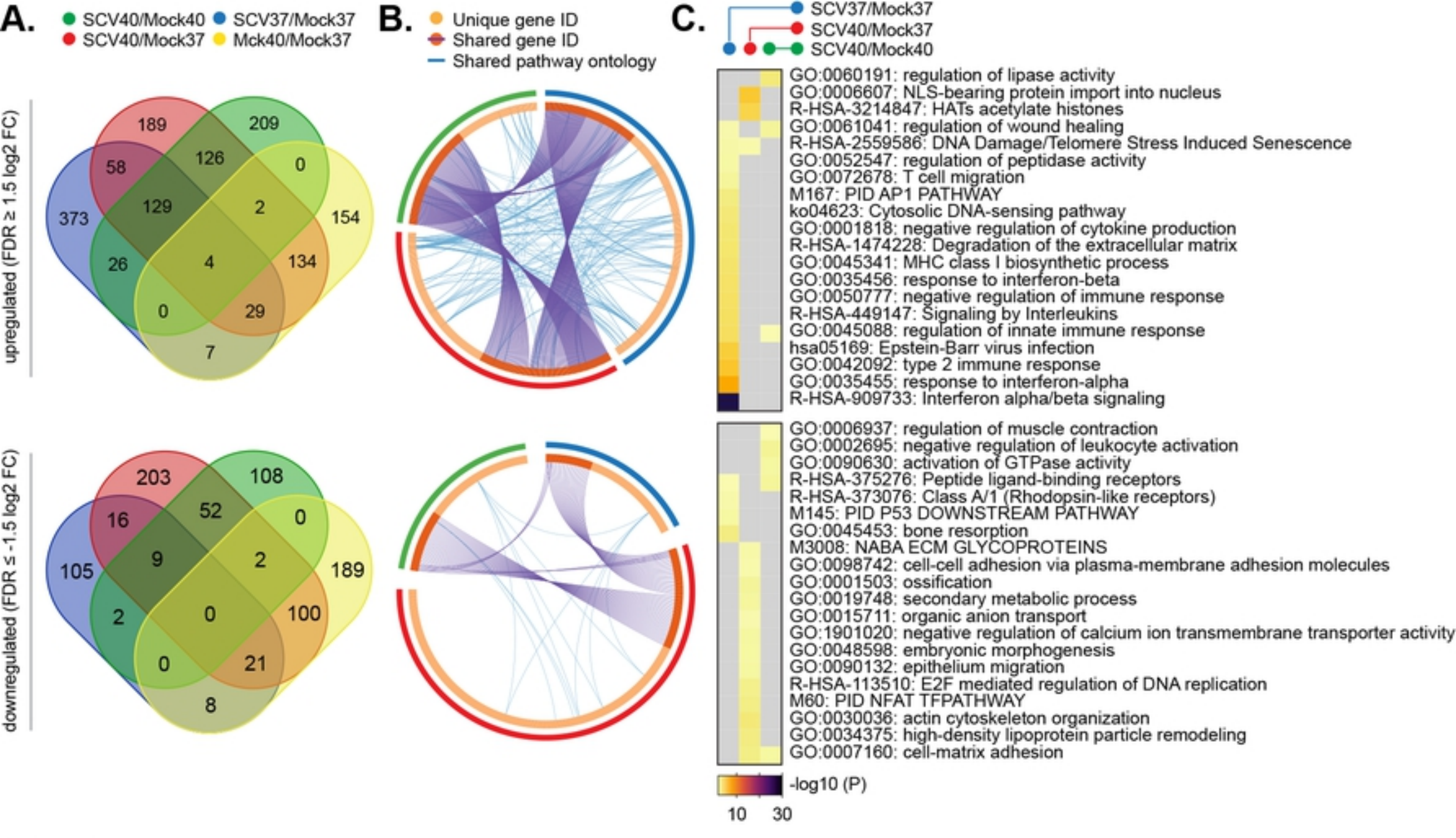
A.
SCV40/Mock40
SCV37/Mock37
SCV40/Mock37
Mck40/Mock37
upregulated (FDR ≥ 1.5 log2 FC)
189
209
58
126
0
373
129
2
154
26
4
134
0
29
7
downregulated (FDR ≤ -1.5 log2 FC)
203
108
16
52
0
105
9
2
189
2
0
100
0
21
8
B.
Unique gene ID
Shared gene ID
Shared pathway ontology
C.
SCV37/Mock37
SCV40/Mock37
SCV40/Mock40
GO:0060191: regulation of lipase activity
GO:0006607: NLS-bearing protein import into nucleus
R-HSA-3214847: HATs acetylate histones
GO:0061041: regulation of wound healing
R-HSA-2559586: DNA Damage/Telomere Stress Induced Senescence
GO:0052547: regulation of peptidase activity
GO:0072678: T cell migration
M167: PID AP1 PATHWAY
ko04623: Cytosolic DNA-sensing pathway
GO:0001818: negative regulation of cytokine production
R-HSA-1474228: Degradation of the extracellular matrix
GO:0045341: MHC class I biosynthetic process
GO:0035456: response to interferon-beta
GO:0050777: negative regulation of immune response
R-HSA-449147: Signaling by Interleukins
GO:0045088: regulation of innate immune response
hsa05169: Epstein-Barr virus infection
GO:0042092: type 2 immune response
GO:0035455: response to interferon-alpha
R-HSA-909733: Interferon alpha/beta signaling
GO:0006937: regulation of muscle contraction
GO:0002695: negative regulation of leukocyte activation
GO:0090630: activation of GTPase activity
R-HSA-375276: Peptide ligand-binding receptors
R-HSA-373076: Class A/1 (Rhodopsin-like receptors)
M145: PID P53 DOWNSTREAM PATHWAY
GO:0045453: bone resorption
M3008: NABA ECM GLYCOPROTEINS
GO:0098742: cell-cell adhesion via plasma-membrane adhesion molecules
GO:0001503: ossification
GO:0019748: secondary metabolic process
GO:0015711: organic anion transport
GO:1901020: negative regulation of calcium ion transmembrane transporter activity
GO:0048598: embryonic morphogenesis
GO:0090132: epithelium migration
R-HSA-113510: E2F mediated regulation of DNA replication
M60: PID NFAT TFPATHWAY
GO:0030036: actin cytoskeleton organization
GO:0034375: high-density lipoprotein particle remodeling
GO:0007160: cell-matrix adhesion
-log10 (P)
10
30

Fig 5

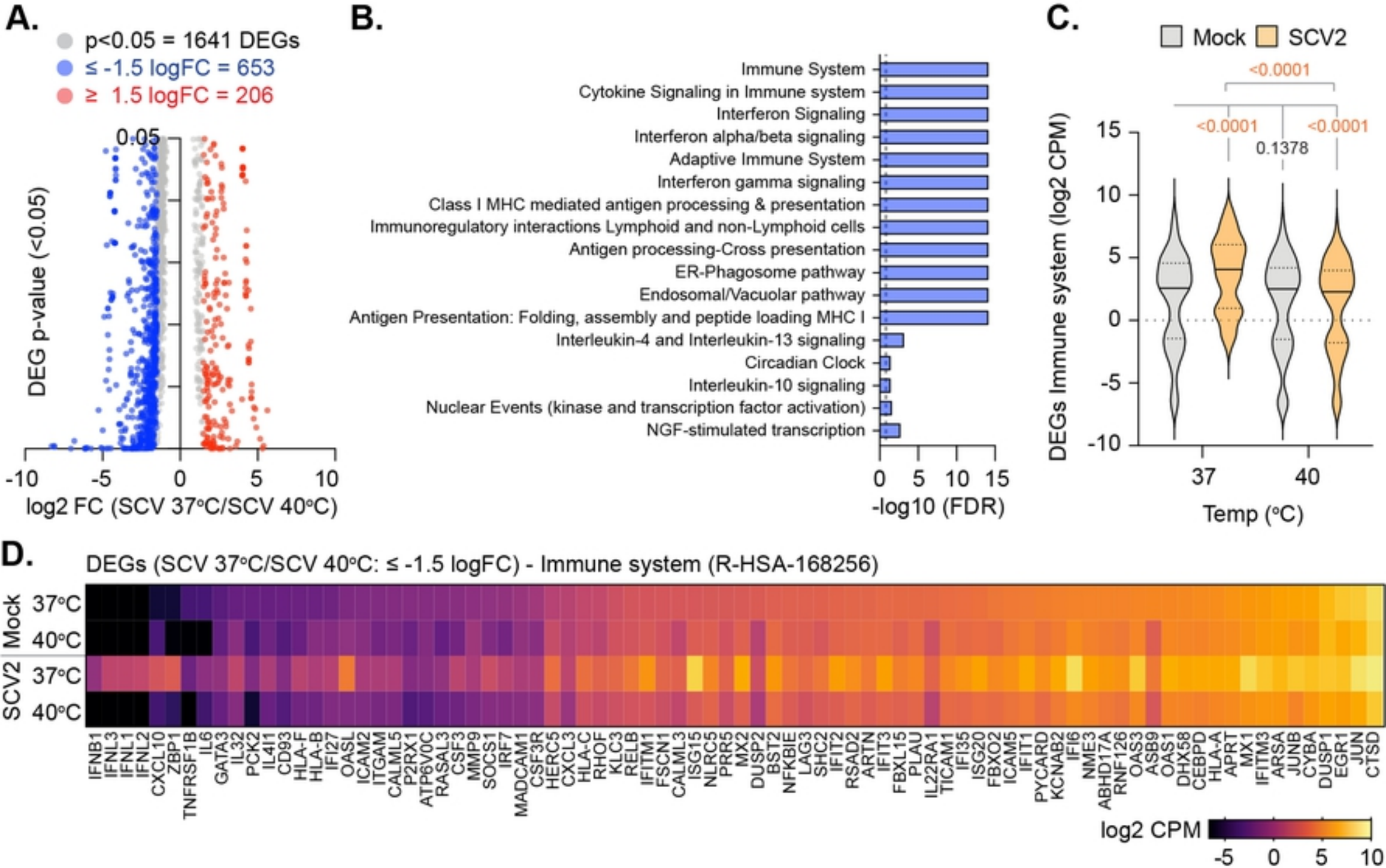
A.
p<0.05 = 1641 DEGs
≤ -1.5 logFC = 653
≥ 1.5 logFC = 206
0.05
DEG p-value (<0.05)
-10
-5
0
5
10
log2 FC (SCV 37°C/SCV 40°C)
B.
Immune System
Cytokine Signaling in Immune system
Interferon Signaling
Interferon alpha/beta signaling
Adaptive Immune System
Interferon gamma signaling
Class I MHC mediated antigen processing & presentation
Immunoregulatory interactions Lymphoid and non-Lymphoid cells
Antigen processing-Cross presentation
ER-Phagosome pathway
Endosomal/Vacuolar pathway
Antigen Presentation: Folding, assembly and peptide loading MHC I
Interleukin-4 and Interleukin-13 signaling
Circadian Clock
Interleukin-10 signaling
Nuclear Events (kinase and transcription factor activation)
NGF-stimulated transcription
0
5
10
15
-log10 (FDR)
C.
Mock
SCV2
<0.0001
<0.0001
<0.0001
0.1378
DEGs Immune system (log2 CPM)
15
10
5
0
-5
-10
37
40
Temp (°C)
D.
DEGs (SCV 37°C/SCV 40°C: ≤ -1.5 logFC) - Immune system (R-HSA-168256)
Mock
SCV2
37°C
40°C
37°C
40°C
IFNB1
IFNL3
IFNL1
IFNL2
CXCL10
ZBP1
TNFRSF1B
IL6
GATA3
IL32
PCK2
IL4I1
CD93
HLA-F
HLA-B
IFI27
OASL
ICAM2
ITGAM
CALML5
P2RX1
ATP6V0C
RASAL3
CSF3
MMP9
SOCS1
IRF7
MADCAM1
CSF3R
HERC5
CXCL3
HLA-C
RHOF
KLC3
RELB
IFITM1
FSCN1
CALML3
ISG15
NLRC5
PRR5
MX2
DUSP2
BST2
NFKBIE
LAG3
SHC2
IFIT2
RSAD2
ARTN
IFIT3
FBXL15
PLAU
IL22RA1
TICAM1
IFI35
ISG20
FBXO2
ICAM5
IFIT1
PYCARD
KCNAB2
IFI6
NME3
ABHD17A
RNF126
OAS3
ASB9
OAS1
DHX58
CEBPD
HLA-A
APRT
MX1
IFITM3
ARSA
JUNB
CYBA
DUSP1
EGR1
JUN
CTSD
log2 CPM
-5
0
5
10

Fig 6

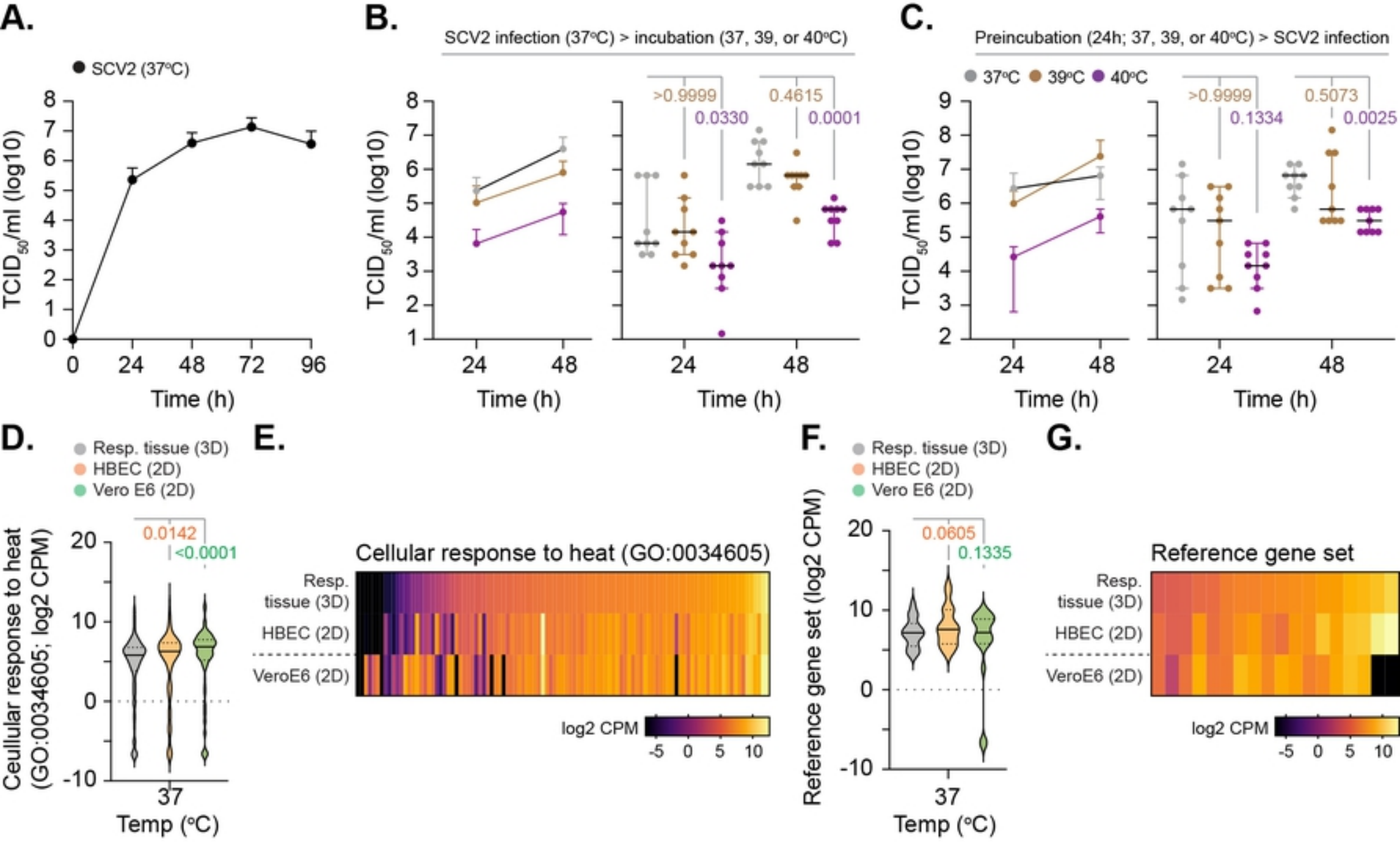
A.
SCV2 (37°C)
TCID50/ml (log10)
Time (h)
B.
SCV2 infection (37°C) > incubation (37, 39, or 40°C)
>0.9999
0.0330
0.4615
0.0001
C.
Preincubation (24h; 37, 39, or 40°C) > SCV2 infection
37°C
39°C
40°C
>0.9999
0.1334
0.5073
0.0025
D.
Resp. tissue (3D)
HBEC (2D)
Vero E6 (2D)
0.0142
<0.0001
Ceullular response to heat (GO:0034605; log2 CPM)
Temp (°C)
E.
Cellular response to heat (GO:0034605)
Resp. tissue (3D)
HBEC (2D)
VeroE6 (2D)
log2 CPM
F.
0.0605
0.1335
Reference gene set (log2 CPM)
G.
Reference gene set

Fig 7

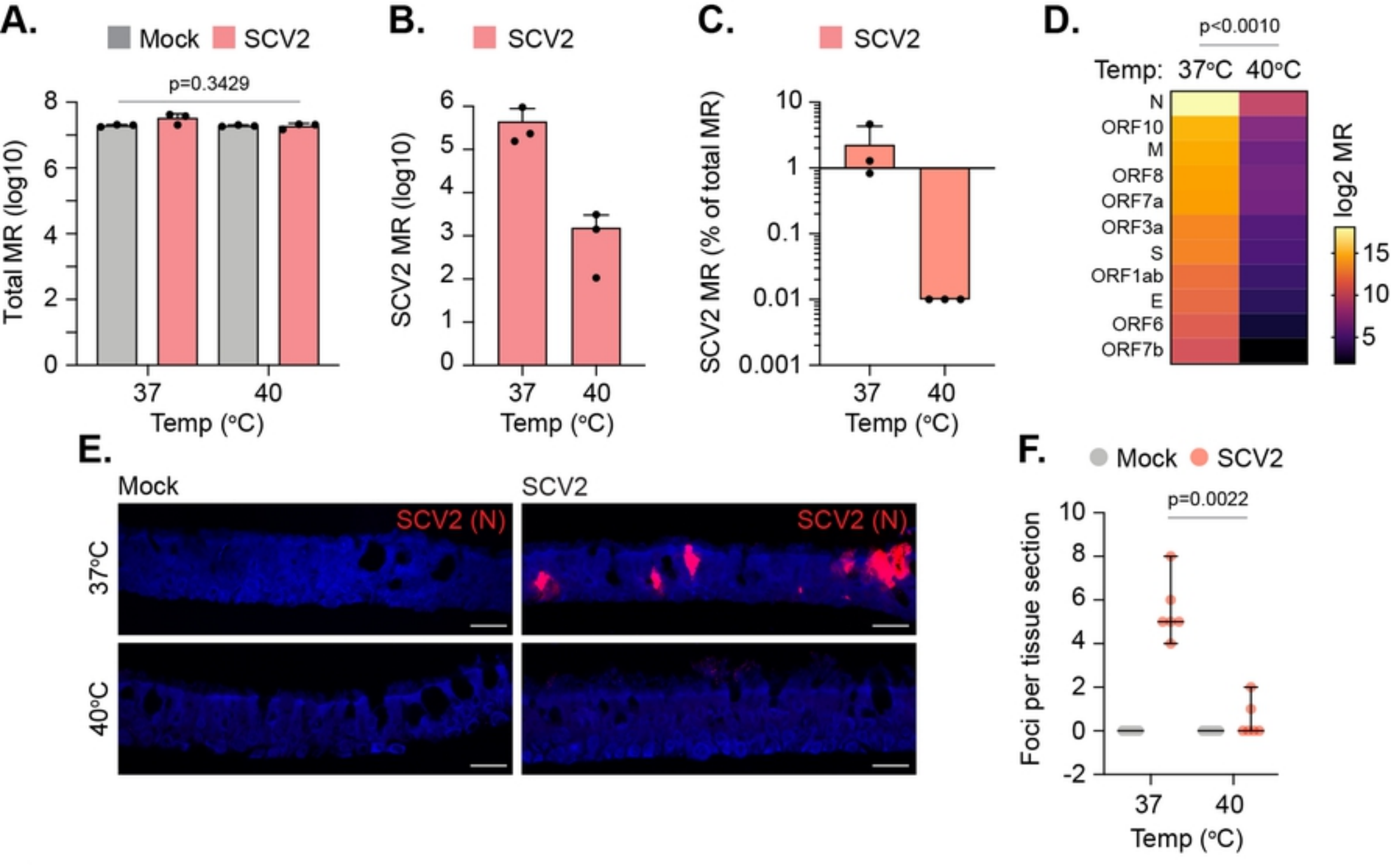
A.
Mock
SCV2
p=0.3429
Total MR (log10)
Temp (°C)
B.
SCV2
SCV2 MR (log10)
Temp (°C)
C.
SCV2
SCV2 MR (% of total MR)
Temp (°C)
D.
p<0.0010
Temp: 37°C 40°C
N
ORF10
M
ORF8
ORF7a
ORF3a
S
ORF1ab
E
ORF6
ORF7b
log2 MR
E.
Mock
SCV2
SCV2 (N)
37°C
40°C
F.
Mock
SCV2
p=0.0022
Foci per tissue section
Temp (°C)

Fig 8